Valence Bond Diagrams

DOI: 10.1002/anie.201108398

Hydrogen-Abstraction Reactivity Patterns from A to Y: The Valence Bond Way

*Wenzhen Lai, Chunsen Li, Hui Chen, and Sason Shaik**

Keywords:
closed-shell abstractors · compound I · hydrogen atom abstraction · proton-coupled electron transfer · valence bond diagrams

In memory of Saul Wolfe

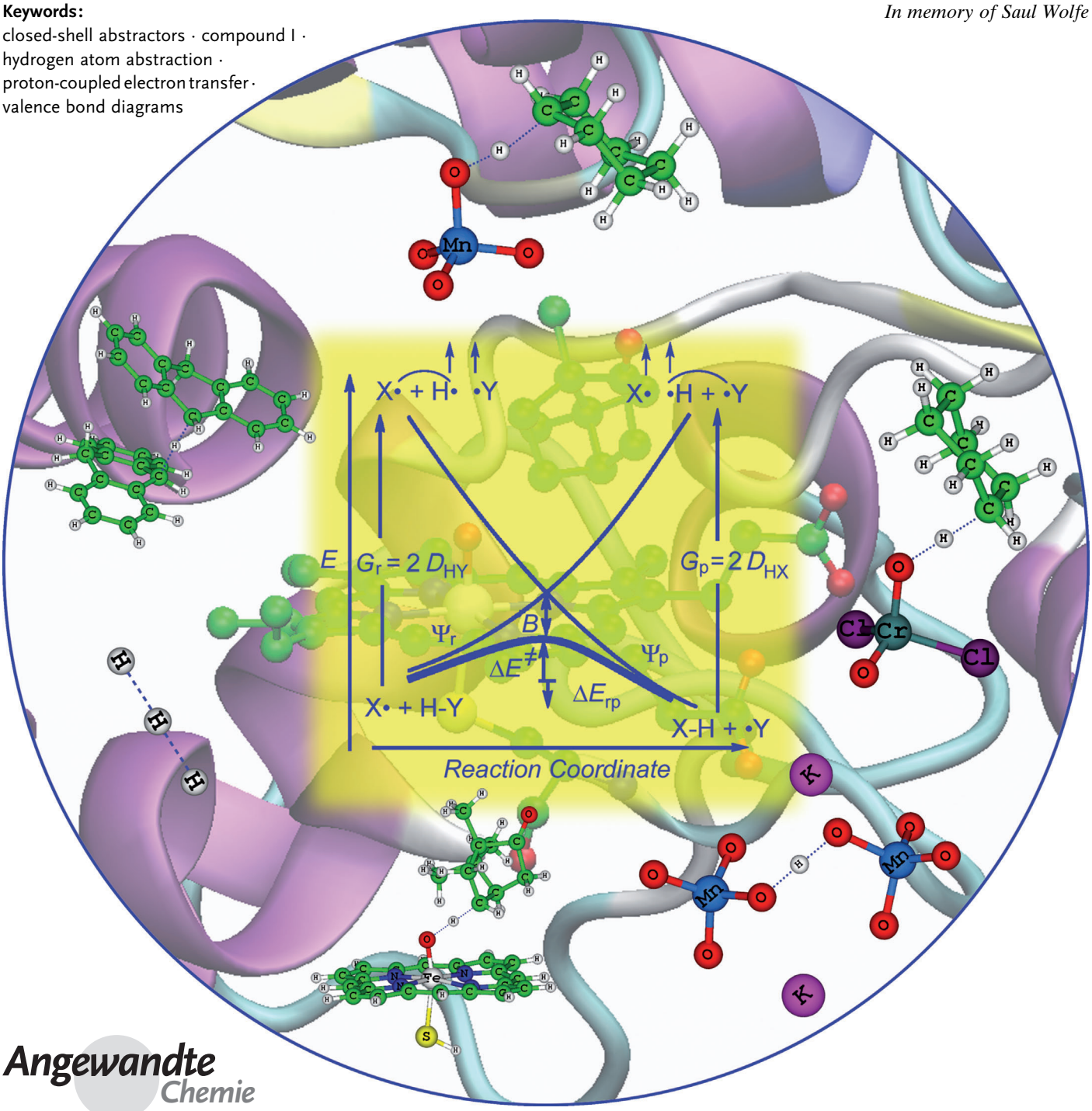

"Give us insight, not numbers" was Coulson's admonition to theoretical chemists. This Review shows that the valence bond (VB)-model provides insights and some good numbers for one of the fundamental reactions in nature, the hydrogen-atom transfer (HAT). The VB model is applied to over 50 reactions from the simplest H + H_2 process, to P450 hydroxylations and H-transfers among closed-shell molecules; for each system the barriers are estimated from raw data. The model creates a bridge to the Marcus equation and shows that H-atom abstraction by a closed-shell molecule requires a higher barrier owing to the additional promotion energy needed to prepare the abstractor for H-abstraction. Under certain conditions, a closed-shell abstractor can bypass this penalty through a proton-coupled electron transfer (PCET) mechanism. The VB model links the HAT and PCET mechanisms conceptually and shows the consequences that this linking has for H-abstraction reactivity.

From the Contents

1. Introduction

Hydrogen-atom abstraction (HAT), Equation (1), is one of the fundamental processes occurring in chemistry. Its understanding is therefore of eminent importance.

$$X^{\bullet} + H{-}Y \rightarrow X{-}H + Y^{\bullet} \quad (1)$$

Indeed, most chemical oxidative processes begin with a hydrogen abstraction (H-abstraction) step.[1] Transition-metal-based enzymes, such as the heme cytochromes P450,[2,3] oxidize a variety of substrates by means of H-abstraction, utilizing the high-valent iron oxo active species ($X^{\bullet}$ = $Por^{+\bullet}Fe^{IV}O$), which is called Compound I (Cpd I), and which performs many metabolic processes, neutralizes xenobiotics, and forms our brain chemicals (e.g., serotonin and dopamine) from trace amines in the brain.[4] Plants build their cell walls by H-abstraction from the O–H bonds of phenols using heme enzymes, such as Horseradish Peroxidase.[5] Cell membranes are disrupted by H-abstraction from lipids, proteins turn plaques when radicals activate them by H-abstraction from N–H and C–H bonds, and this is also the manner in which DNA is damaged and other biologically important processes occur.[6] Similarly, non-heme iron enzymes catalyze an array of oxidative conversions, which all commence with H-abstraction by the reactive iron oxo species ($X = L_nFe^{IV}O$) of these enzymes.[7] The interest in these enzymes has caused the field of bioinorganic chemistry to flourish,[7a] and many synthetic metal oxo complexes,[1,7c,d,8] and small diatomic analogues[9] have been prepared and tested for their ability to abstract hydrogen atoms. Many catalytic C–H bond activation reactions are initiated[9c,10] by H-abstraction from the alkane. Moreover, H-abstractions also transpire during combustion of hydrocarbons, in industrial hydrocarbon oxidations,[11] and in atmospheric processes.[12] The list is indeed endless, attesting to the importance of H-abstraction and to the dimension of the task lying ahead to comprehend these data.

In many of these H-abstraction reactions it is necessary or preferable to have a radical center on the abstractor, be it a simple radical, a radical cation,[13] or a metal oxo compound, such as the high-valent Fe^{IV}=O species that is common to heme and non-heme enzymes, and which has an oxyl-radical character,[14] as well as in "main-group-element catalysts" such as P-O$^{\bullet}$, Pb-O$^{\bullet}$, Ge-O$^{\bullet}$, Al-O$^{\bullet}$, species.[15] However, it has been shown in the early 1960s,[16] that closed-shell CrO_2Cl_2 and chromic acid oxidize alkanes, most likely by means of H-abstraction. Indeed, as was demonstrated recently,[17–20] H-abstraction reactions can be initiated also by closed-shell molecules. For example, closed-shell metal-oxo species, such as CrO_2Cl_2 or MnO_4^-,[17–19] or olefins, such as α-methylstyrene,[18] can abstract H from alkanes, even though the H-abstractors have no unpaired electrons. Such a reaction is the Ètard oxidation, Equation (2), which was unequivocally

[*] Dr. W. Lai,[+] Dr. C. Li,[+] Prof. Dr. H. Chen, Prof. Dr. S. Shaik
Institute of Chemistry and the Lise-Meitner-Minerva Center for Computational Quantum Chemistry, The Hebrew University of Jerusalem
91904 Jerusalem (Israel)
E-mail: sason@yfaat.ch.huji.ac.il
Dr. W. Lai[+]
Department of Chemistry, Renmin University of China
Beijing, 100872 (China)
Prof. Dr. H. Chen
Beijing National Laboratory for Molecular Sciences (BNLMS), CAS Key Laboratory of Photochemistry, Institute of Chemistry, Chinese Academy of Sciences
Beijing, 100190 (China)
[+] These authors contributed equally to this work.

Supporting information for this article is available on the WWW under http://dx.doi.org/10.1002/anie.201108398.

demonstrated,[16,17a,b,19] to start by H-abstraction leading to the formation of two radicals.

$$Cr^{VI}O_2Cl_2 + H\text{-}Alk \rightarrow Cr^{V}{}^{\bullet}OCl_2(OH) + Alk^{\bullet} \rightarrow\rightarrow \text{ products} \quad (2)$$

Recently the notion of closed-shell abstractors has become a hot topic, with reports on the efficient H-abstraction reactivity of $Mn^{V}O$ and $Ru^{IV}O$ in their singlet states.[21] In view of the debate on the report on $Ru^{IV}O$ reactivity,[22] the fact that in most known $Mn^{V}O$ systems the reactive state is not the closed-shell singlet but rather the open-shell states,[14a–c,23,24] and the recent report that the closed-shell abstractor vanadium(V) oxo species is more sluggish than an analogous open-shell abstractor $Ru^{IV}O$,[25] it is deemed clearly important to outline the relationship between the open-shell and closed-shell H-abstraction types.

Another surging topic is the finding that quite a few of the HAT reactions occur through the alternative path of *concerted* proton-coupled electron transfer (PCET),[26,27] which involves a proton abstraction by the abstractor atom center, while at the same time relaying the odd electron through an orbital that is not involved in the X-H-Y axis. What is then the relationship between "normal" HAT and PCET?

In brief, H-abstraction is a ubiquitous reaction that involves intriguing features. But how do we understand all this rich chemistry using a single unifying theory?

1.1. Introduction of the Marcus Equation

In the past decade or so, Mayer[28] has shown that the Marcus equation,[29] Equation (3a), provides a general treatment of H-abstraction reactivity in terms of the interplay of an intrinsic barrier ($\Delta G^{\neq}_0$) and a thermodynamic driving force (ΔG_{rp}). The thermodynamic driving force factor is related to the Bell–Evans–Polanyi (BEP) principle, which predicts lower barriers for more exothermic processes.[30]

$$\Delta G^{\neq}_{XY} = \Delta G^{\neq}_0 + 0.5\,\Delta G_{rp} + \Delta G_{rp}{}^2/[16\,\Delta G^{\neq}_0] \quad (3a)$$

$$\Delta G^{\neq}_0 = {}^1\!/_2[\Delta G^{\neq}_{XX} + \Delta G^{\neq}_{YY}] \quad (3b)$$

It is occasionally stated that the Marcus equation is strictly correct only for electron transfer reactions (zero overlap regime), and that it is derived from a model of two intersecting parabolas. In fact, however, Murdoch[31] showed that Equation (3a) reflects simply that a barrier can generally be dissected into an intrinsic kinetic term and a thermody-

Wenzhen Lai received her B.Sc. (2002) in chemistry and her M.Sc. (2005) in physical chemistry from Sichuan University. In 2008 she obtained her Ph.D. in theoretical and computational chemistry from Nanjing University with Prof. Daiqian Xie. After postdoctoral research (2008–2011) at the Hebrew University in the group of Prof. Sason Shaik, she joined Department of Chemistry, Renmin University of China, as an associate professor and principle investigator. Her main research interests are theoretical studies of homogeneous and heterogeneous catalysis by metal-containing systems.

Chunsen Li received his B.Sc. in chemistry (2001), M.Sc. (2004), and Ph. D. (2007) in physical chemistry from Xiamen University, China, with Prof. Wei Wu. Subsequently he joined the group of Prof. Walter Thiel at the Max-Planck-Institut für Kohlenforschung in Mülheim an der Ruhr, Germany, as a postdoctoral fellow (2008–2010). He is currently working with Prof. Sason Shaik as a postdoctoral fellow at the Hebrew University. His main research interests are QM and QM/MM studies of the mechanism and catalysis of heme and non-heme systems.

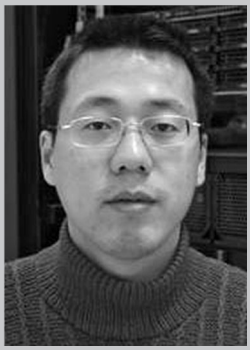

Hui Chen received his B.Sc. (2001) in chemistry and Ph.D. (2006) in physical chemistry both from Nanjing University in China, on a theoretical study of excited states of organic molecules with Prof. Shuhua Li. He then worked with Prof. Sason Shaik as a postdoctoral fellow at the Hebrew University, where he won the Lise Meitner Prize of the Lise-Meitner-Minerva Center (2007) for computational quantum chemistry. In 2011, he joined the Institute of Chemistry, in the Chinese Academy of Sciences (ICCAS), to start his independent research. His current main research interests include intriguing reaction mechanisms and complex electronic structures of both ground and excited states in chemistry and biochemistry.

Sason Shaik has obtained his Ph. D from the University of Washington with Nicolaos D. Epiotis (1978). After a postdoctoral year with Roald Hoffmann he started his first academic position as a Lecturer at Ben-Gurion University (BGU) where he became Professor in 1988. In 1992 he moved to the Hebrew University, and together with Yitzhak Apeloig has established the Lise Meitner Minerva Center, which he has been directing ever since. Among the awards he has received are the Lise-Meitner-Alexander von Humboldt Senior Award in 1996, the Kolthoff Award, and the Israel Chemical Society Prize (2001), in 2005 he was made Fellow of the AAAS, and received the 2007 Schrödinger Medal of WATOC. Recently he has been chosen for the Frontier Lectureship Award of the Max Planck Institute of Bioinorganic Chemistry in Mülheim. In August 2012, he will receive, jointly with Martin Quack, the August Wilhelm von Hofmann Medal of the German Chemical Society.

namic driving force term (see Supporting Information for such derivation of Equation (3a)). Marcus himself has derived the expression for HAT reactions using the bond-energy bond-order (BEBO) approach.[29b]

The validity of the averaging approximation in Equation (3b) has been amply discussed; for example, it was justified from transferability principles of fragments from one molecular species to the other.[32] Transferability is the basis of notions of substituent effects and of average bond energies, and although this is only an approximation, it is quite a good one. As such, Equation (3) is a useful rate-equilibrium relationship tool for analyzing experimental barrier data. Indeed, the Marcus equation has been successfully applied to a variety of reactions, starting from electron transfer and going to group transfers.[33]

Mayer's work[28] has demonstrated that the equation is satisfied for H-abstraction reactions over many orders of magnitude in experimental rate constants, and that cases, where the BEP principle breaks down, arise from changes in the intrinsic barrier (or intrinsic rate constant). This is a major achievement, albeit requiring a significant effort. Thus, as specified in Equation (3b), the intrinsic barrier $\Delta G^{\neq}_{0}$ is determined as an average of the two identity barriers, where the abstractor, X$^{\bullet}$ in Equation (1), abstracts a hydrogen atom from H–X, and Y$^{\bullet}$ abstracts a hydrogen atom from H–Y. As such, although the Equation (3) is a fabulously compact expression for dissecting the barrier into its building blocks, it still requires the investigator to determine the barriers or the rate constants of two identity reactions, in addition to the reaction of interest. This situation means that the understanding of the barrier $\Delta G^{\neq}_{XY}$ in Equation (3a) must rely on the quantity $\Delta G^{\neq}_{0}$, which itself is made of two barriers that may or may not always be understood, for example, why should $\Delta G^{\neq}_{XX}$ be smaller or larger than $\Delta G^{\neq}_{YY}$ in a given case? Thus it is desirable to develop a model that allows estimations of $\Delta G^{\neq}_{XY}$ and $\Delta G^{\neq}_{XX}$ and/or $\Delta G^{\neq}_{YY}$ *from raw accessible data*, and this is the main focus of this Review.

1.2. Goals and the Valence Bond Diagram Model

An approach that can achieve these goals is based on the valence bond (VB) diagram model, which has been amply applied to HAT.[34] The model provides a unified view of chemical reactivity,[35] which has been broadly applied to organic reactions,[35c,36] homogeneous catalysis,[37] and excited-state reactivity.[38] Very recently, the Jerusalem group[39] has extended the VB model to treat reactions of P450, such as H-abstraction, arene activation, and sulfoxidation. Similarly, the Manchester group[40] has applied the model to non-heme H-abstractions and to epoxidation reactions by P450. Importantly, these applications have shown that the VB model is capable of evaluating H-abstraction barriers and deriving general trends from accessible raw data, such as bond energies.[39a,b] Note however, that VB approaches to reactivity are immensely useful in many other areas[41–43] that are not covered herein.

Herein we demonstrate the generality and unifying power of the VB model for understanding H-abstraction reactivity starting from the simplest $H + H_2$ process, through organic and main-group-element reactions and all the way to P450 hydroxylations and H-transfer among closed-shell molecules; altogether well over 50 reactions, which are collected in groups in Scheme 1.

In Scheme 1 a are simple radicals, X$^{\bullet}$ and Y$^{\bullet}$ for which both identity (X = Y) and nonidentity (X ≠ Y) reactions are considered. Scheme 1 b shows reactions that were studied by experimental means. Scheme 1 c includes the P450 series of Cpd I with a variety of alkanes, while Scheme 1 d includes H-abstractions by closed-shell metal oxo abstractors, and

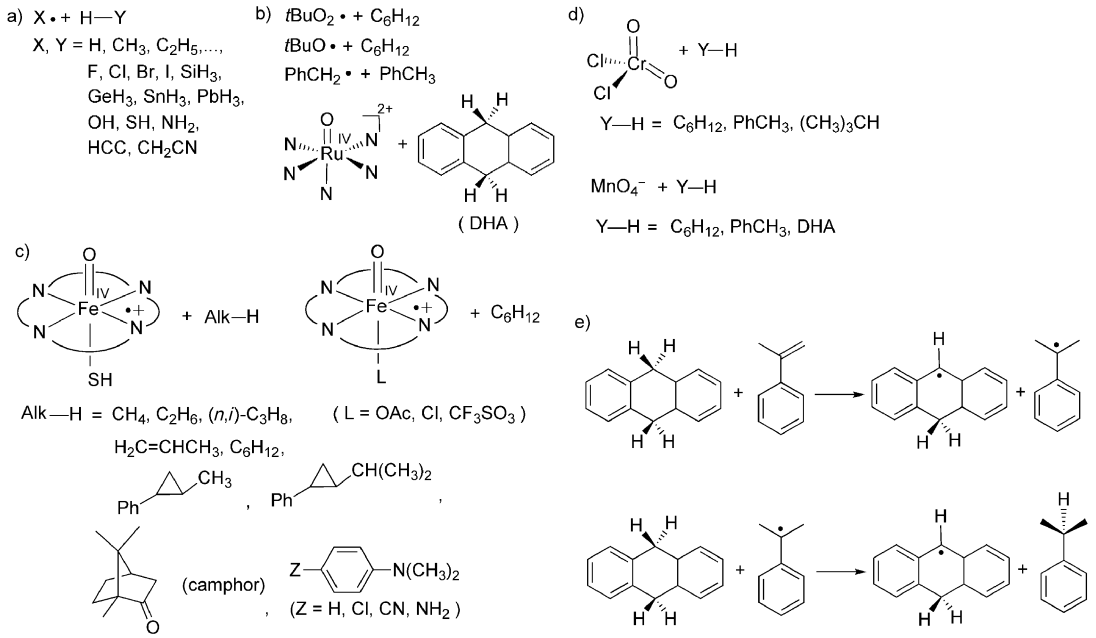

Scheme 1. H-abstraction reactions used for application of the VB Model.

Scheme 1e shows H-abstraction using closed-shell molecules and for analogous reactions using a radical abstractor. The barriers of the reactions in Scheme 1a were calculated for this Review using the coupled cluster CCSD(T) method with complete basis set (CBS) estimates, hence CCSD(T)/CBS (see details in the Supporting Information), which compare well with experimentally determined barriers.[44] Other barriers, such as those in Scheme 1c were studied before[39a,b] with DFT using the B3LYP functional and the LACV3P++* basis set. For other reactions from Scheme 1b,d, and e, we simply derived VB barriers that could be compared with experimental barriers, using experimental as well as UB3LYP calculated bond dissociation energies (BDEs) and other necessary quantities. To test the VB predictions of intrinsic barriers, we also studied a few new reactions; the self-exchange reactions of $MnO_4^-/MnO_3(OH)^{\bullet-}$ and of the 9-hydroanthrace radical (DHA(-H$^\bullet$)) with 9,10-dihydroanthracene (DHA), as well as of the reaction of MnO_4^- with cyclohexane (C_6H_{12}), using B3LYP/LACV3P++**// LACVP** (see the Supporting Information). In the following text, we label the basis sets LACV3P++** as B1, and LACV3P++* as B2.

One of our goals herein is to show that H-abstraction barriers can be reasonably estimated from raw and easily accessible data. Another goal is to enable the estimation of intrinsic barriers from these raw data and thereby create a direct bridge to the Marcus equation, and to its experimentally determined identity barriers. Another wishful bridge is between the HAT and PCET mechanisms. Lastly, we also explore the ability of the model to predict, from raw data, experimentally known barriers for a variety of HAT and PCET reactions.

Thus, we intend to show that the model enables questions, such as, "do we really need radicals to abstract hydrogen atom?" to be answered. It will be argued that in such comparisons, the correct question is, "*what is the energetic cost of creating radical at the abstractor site, and whether there is a way that a closed-shell abstractor might avoid creating such a radical center in the transition-state region and at the same time still abstract a hydrogen atom*?"[35c] It will be shown that PCET is such a mechanism that avoids the penalty of creating a radical during reactions of closed-shell abstractors. Finally, the VB diagram will outline the relationship between normal HAT and the alternative PCET path, and will demonstrate that the HAT–PCET characters are generally mixed and form a mechanistic spectrum of cases between the two limits. The PCET character in a HAT process will be shown to depend on the bond energy of the H-donor molecule H–Y, and the ionization energy of the abstractor X (or X$^\bullet$) and of the Y$^\bullet$ radical [Equation (1)].

In the Review we will also assess the limitations of the VB model. One of these limitation is that in its present form, it does not allow rate constants (or free energy barriers) to be calculated, another limitation is that the model does not consider tunneling, which is very important in H-abstraction reactions.[44d,45] But as we hope to demonstrate, the advantages of the model are clear and they outweigh the limitations.

2. The Valence Bond Model of Chemical Reactivity

The VB diagram model was developed in 1981 with the aim of building up energy profiles from individual VB "building blocks" and creating thereby VB state correlation diagrams based on VB presentation of the states.[35a] We emphasize that the VB diagram is not a random curve crossing model. It is based on first principles of electronic structure and was derived by mapping MO-based states onto VB structures,[35a,e] and was corroborated by numerous ab initio quantum chemical studies.[34,46,47]

Figure 1a shows the generic VB diagram, so-called, the VB state correlation diagram (VBSCD)[35c,48] that provides a mechanism for the barrier formation and generation of

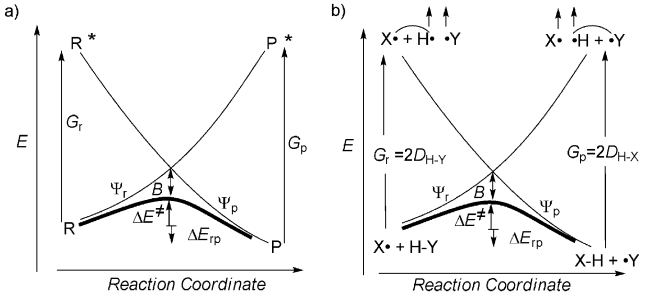

Figure 1. a) A generic VB state correlation diagram (VBSCD) model. R* and P* are the image (prepared) states of the ground states (R and P) with which the image (prepared) states correlate. b) VBSCD for the simple H-abstraction reaction X$^\bullet$ + H–Y → X–H + $^\bullet$Y. The arched lines connecting the electrons of the excited states signify that these electrons are spin-paired (to a singlet state) and will become bonded at the corresponding ground state at the bottom of the state curve.

a transition state (TS) in an elementary reaction. In this case, two state curves describing reactant- and product-bonding interchange along the reaction pathway, and by mixing they lead to a transition state and a barrier that separate reactants and products. The two state-curves are anchored in the ground states of the reactants and products (R and P), and in two excited states (R* and P*), which are the so-called "electronic image" states, or synonymously the "prepared states"[35a,e] of the ground states with which they correlate. Figure 1b shows the VB diagram for an elementary HAT. It is clearly seen, that the bonds that undergo activation, on both reaction sides, are prepared for bonding changes in the "image states" by triplet decoupling of the bond electrons and re-coupling them with the distant radical (for PCET and for H-abstraction between closed-shell molecules, see Section 5).

2.1. The VB Barrier Expressions

Let us clarify the key states and the reactivity parameters in the VBSCD in Figure 1a. In the image state R*, we undo the pairing of the electrons in the bonds of R that have to be broken during the reaction, while re-coupling the electrons as in P, into new bond pairs. When predictions of reaction trajectories are essential, the symmetry-matched fragment

orbitals should be used to occupy these electrons.[35a,d,e] Similar considerations apply to P* and naturally to P. Thus, R* is the electronic image of P in the geometry of R, while P* is the image of R at the geometry of P. The G terms are the corresponding *promotion energy gaps*, B is the resonance energy of the transition state, $\Delta E^{\neq}$ is the energy barrier, and ΔE_{rp} is the reaction energy.

The simplest barrier expression is [Eq. (4)].

$$\Delta E^{\neq} = f\,G_r - B \tag{4}$$

The term fG_r in Equation (4) gauges the height of the crossing point above the reactant state, expressed as some fraction (f) of the promotion gap at the reactant side (G_r). Hence, fG_r constitutes the total distortion and repulsion energies required to bring R to the crossing point into resonance with P, while B is the corresponding resonance energy stabilization of the transition state. Obvious affinity exists in this case with the "activation strain model" that is based on energy decomposition analysis of the barrier.[47,49–51] Equation (4) provides a very useful expression, which can be applied to "reaction families"[35c,d,e,48] wherein both f and B are constants (quasi-constants), as was indeed found in a few cases including the reactivity of P450 Cpd I in alkane hydroxylation where $f = 0.3$ and $B = 46.78\ \text{kcal mol}^{-1}$ gave quite satisfactory results.[39a,b]

Our goal however, is to model H-abstraction reactivity of many unrelated reactions (Scheme 1), in which we know that B is not a constant. Additionally, our wish to link the VB model to the Marcus equation and the BEP principle cannot be achieve explicitly with Equation (4). For these more ambitious goals we are going to use the explicit barrier expression, in Equation (5a). This expression shows the

$$\Delta E^{\neq} \approx f_0\,G_0 + 0.5\,\Delta E_{rp} + 0.5\,[\Delta E_{rp}{}^2/G_0] - B \tag{5a}$$

dependence of the barrier on the thermodynamic driving force, ΔE_{rp}, as well as on the two different promotion gaps (G_r and G_p) and f factors using their averages in Equation (5b).[34f,35c,e,39b,48] Note however, that whenever the ΔE_{rp} term is

$$G_0 = 0.5(G_r + G_p), \qquad f_0 = 0.5(f_r + f_p) \tag{5b}$$

much smaller than the averaged promotion gap, G_0, the barrier expression can be simplified to Equation (5c). Further, it is seen that either Equations (5a) or (5c) lead to a simple expression for the intrinsic barrier, in Equation (5d).

$$\Delta E^{\neq}{}_0 \approx f_0\,G_0 - B \tag{5c}$$

$$\Delta E^{\neq}{}_0 \approx f_0\,G_0 - B \tag{5d}$$

As in Equation (4), the $f_0 G_0$ term gauges the total deformation and repulsive energies of the reactant and product moieties in the transition state, while ΔE_{rp} modulates this quantity, by decreasing/increasing the deformation for an exothermic/endothermic reaction. And finally, B is the resonance energy stabilization of the transition state owing to delocalization of the active electrons over the X-H-Y moieties. What we have to do now is to convert G_0, B, ΔE_{rp}, and f_0 into quantities that could either be accessed from experimental data or from easily calculated data. As shown in the next Section, this is achievable for H-abstraction.

2.1.1. Simple H-Abstractions and VB-Based Barrier Expressions

Figure 1b above shows the VBSCD for an elementary H-abstraction step by a radical X•. As already noted, the "image" states R* and P* are "prepared" by de-coupling the bonds, H–Y and X–H, of the ground states, into triplets while newly spin-pairing the electron of H• to the other radicals, X• and Y•, respectively. Based on semi-empirical VB expressions, it has been shown before[34,35] that the promotion gap, that is proportional to the singlet–triplet promotion energy[52] (See the Supporting Information, Section VB) of the bonding electrons of a bond, can be expressed as two times *the vertical bond strength D*;[39a,b] the vertical bond strength measures the strength of the interaction without allowing the radicals to relax to their preferred geometry when free. A vertical quantity that measures the strength of the interaction between the H–X or Y–H fragments is required since the excited states in the VBSCD are vertical states of the ground state below them. A reasonable way to approximate D is given by Equation (6).

$$G_r = 2\,D_{H\text{-}Y} = 2\,[\text{BDE}_{H\text{-}Y} + |\text{RE}_{Y\cdot}|] \tag{6a}$$

$$G_p = 2\,D_{H\text{-}X} = 2\,[\text{BDE}_{H\text{-}X} + |\text{RE}_{X\cdot}|] \tag{6b}$$

BDE is the corresponding bond dissociation energy, while, for example, $|\text{RE}_{X\cdot}|$ is the absolute magnitude of the reorganization energy of the X• radical from its optimum structure to its geometry in the H–X molecule. This is an important quantity that will be large for delocalized radicals and small for localized ones. As such, the average promotion gap, G_0, for the VBSCD of the H-abstraction reaction in Figure 1b becomes the sum of the vertical bond strengths of the bonds undergoing activation in the forward and reverse directions [Eq. (7)].

$$G_0 = D_{H\text{-}Y} + D_{H\text{-}X} \tag{7}$$

Thus, the sum of the vertical bond energies will gauge the total deformation energies of the reactants and products, needed to achieve a transition state. The thermodynamic driving force, in Equations (5a) and (5c), is simply the difference of the corresponding BDEs [Eq. (8)].

$$\Delta E_{rp} = \text{BDE}_{H\text{-}Y} - \text{BDE}_{H\text{-}X} \tag{8}$$

Based on the same semi-empirical VB approach, the value of f_0 was shown to be well approximated as 0.3 (see VB section in the Supporting Information).[52b] The Supporting Information shows that either $f_0 = 0.3$ or $f_0 = 1/3$ will predict the trends in the barriers equally well, but the use of $f_0 = 0.3$ yields values closer to zero-point energy (ZPE) corrected barriers, and as such it is used herein.

The semi-empirical VB analysis showed also that the transition-state resonance energy B for an identity reaction where X = Y, could be estimated as one-half of the respective BDE (see the Supporting Information).[34c,f,52b,53] By using BDE we take into account the partial relaxation of the X and Y moieties in the transition state. For a non-identity reaction $X \neq Y$, the semi-empirical VB derivations indicate that B should depend on both bonds in the X-H-Y transition state. Thus, as done before,[53b,c] we use the expressions in Equation (9a).

$$B_{XHY} = {}^1\!/_4\,[BDE_{H\text{-}X} + BDE_{H\text{-}Y}] \quad (9a)$$

$$B_{XHY} = {}^1\!/_2\,BDE_w \quad (9b)$$

The expression in Equation (9b) that was used recently,[34f,39b] equates B_{XHY} to half the BDE of the weaker of the two bonds (BDE_w). This expression was tested herein again and the corresponding barriers are given in the Supporting Information (see, Tables S2 and S7, and Figures S1–S4). Herein, we prefer Equation (9a) which is more elegant, and which reduces naturally to the corresponding expression for the identity reactions. Hence, Equation (9a) treats the identity and non-identity reactions of X and Y on an equal footing, and makes a bridge to the Marcus intrinsic barrier as an average of the corresponding intrinsic barriers [Eq. (5d)].

Plugging the relationships for G_0, ΔE_{rp}, and B [Eqs. (7), (8), and (9a)] and the value of f_0 into Equations (5a), (5c), and (5d), we get the following expressions for the barriers [Eq. (10)].

$$\Delta E^{\neq}{}_{VB}(1) \approx 0.3\,G_0 + 0.5\,\Delta E_{rp} - B_{XHY};\quad G_0 = D_{H\text{-}Y} + D_{H\text{-}X};\quad B_{XHY} = {}^1\!/_4\,[BDE_{H\text{-}X} + BDE_{H\text{-}Y}] \quad (10a)$$

$$\Delta E^{\neq}{}_{VB}(2) \approx \Delta E^{\neq}{}_{VB}(1) + 0.5\,[\Delta E_{rp}{}^2/G_0] \quad (10b)$$

$$\Delta E^{\neq}{}_{VB,0} \approx 0.3\,[D_{H\text{-}Y} + D_{H\text{-}X}] - {}^1\!/_4\,[BDE_{H\text{-}X} + BDE_{H\text{-}Y}] \quad (10c)$$

Thus, Equation (10a) will yield $\Delta E^{\neq}{}_{VB}(1)$ barriers without the quadratic term $0.5[\Delta E_{rp}{}^2/G_0]$, while Equation (10b) will include this term. Equation (10c) will provide the corresponding intrinsic barriers. Using the expressions of the various terms in Equations (6)–(9), Equations (10a)–(10c) could be condensed further; for example, the intrinsic barrier in Equation (10c) would become, $\Delta E^{\neq}{}_{VB,0} \approx 0.05\,[BDE_{H\text{-}X} + BDE_{H\text{-}Y}] + 0.3\,[|RE_{X\cdot}| + |RE_{Y\cdot}|]$. However, at this point we prefer to conserve the form of Equations (10a)–(10c) and emphasize thereby their origins from a state correlation diagram. Note that Equations (10a)–(10c) allow estimation of barriers for any simple H-abstraction using only raw data of bond strengths.

3. Predicting H-Abstraction Reactivity of Simple Radicals

3.1. General Performance of the VB Model

Figure 2 shows the correlations of $\Delta E^{\neq}{}_{VB}(1)$ and $\Delta E^{\neq}{}_{VB}(2)$ [Eq. (10a), (10b)], with the CCSD(T)/CBS and B3LYP/B2 calculated quantities ($\Delta E^{\neq}{}_{calcd}$) for a set of 45 out of the 47 reactions corresponding to those in Scheme 1 a,c. Two reactions were removed, $F^{\cdot} + H_2$ and $I^{\cdot} + HI$, the first is very exothermic and has a negligible CCSD(T)/CBS barrier (0.67 kcal mol^{-1}) while Equation (10b) predicts a negative barrier of -1.9 kcal mol^{-1}. The second has a negative CCSD(T)/CBS barrier that seems to us incorrect.[54] Our VB-estimated barrier for the latter reaction is positive. It might be that getting a positive CCSD(T)/CBS barrier for this reaction requires relativistic treatment with spin orbit coupling explicitly included.

It is seen from Figure 2 that the correlation coefficients for the 45 barriers calculated with Equations (10a) and (10b) are $R^2 = 0.869$ and 0.902, respectively (the correlation using $B = 0.5\,BDE_w$ has $R^2 = 0.903$, see Figure S2), while adding the two omitted cases the R^2 values are 0.818 and 0.876, respectively. The correlation coefficients could improve up to $R^2 = 0.967$ and 0.965 (see Supporting Information Figure S4) if we were to consider only the reactions in Scheme 1 a, while excluding the P450 reactions. This is no wonder since the first set

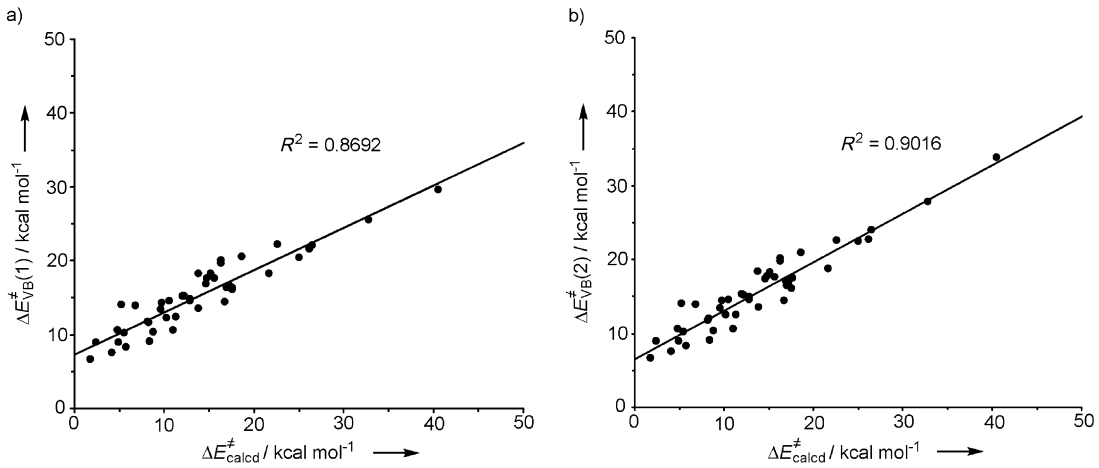

Figure 2. Plots of a) $\Delta E^{\neq}{}_{VB}(1)$ and b) $\Delta E^{\neq}{}_{VB}(2)$ versus the calculated barriers ($\Delta E^{\neq}{}_{calcd}$) using CCSD(T)/CBS for the simple radicals in Scheme 1 a and B3LYP/B2 for the P450 reactions in Scheme 1 c.

involves CCSD(T)/CBS data while the P450 set is calculated with DFT. Still it is important to recognize that the BDE and D values in Equations (10a)–(10c) are variables that represent the promotion gap, and as such, the equation will produce barriers that are gauged by the particular values of the variables, irrespective of their method of determination. It is therefore perfectly legitimate to use the entire set of data for the VB predictions. Clearly, while the correlation coefficients in Figure 2 a,b are not perfect, still considering the range of reactions, these are good correlations that project the usefulness of the VBSCD model.

3.2. VB Modeling of Identity Barriers

To illustrate how to apply the model and to assess its performance and insights for specific cases, we collected a few identity reactions, for which there are either experimental barriers[55,56] or high-level calculated barriers (CCSD(T)/CBS in this study, and MP2/CBS in other studies,[57] or classical barriers without ZPE corrections,[44] and sometimes DFT calculated barriers).[27a] These are collected in Table 1 along with the VB predicted barriers based on BDE(D) values from CCSD(T)-CBS/experimental data unless noted otherwise.[58] Generally, it is seen from the data in the last three columns of Table 1 that the VB-predicted barriers are close to experimental and high-level calculated barriers; the maximum deviation is for X = OH (ca. 3.5 kcal mol^{-1}) in Entry 8. Entry 8 also shows that tunneling will be an important factor that can slice observed barriers by as much as around 4 kcal mol^{-1},[45,57] and this effect is not considered in the VB scheme, as such, and neither in the Marcus equation. A general message from the Table is that the use of experimental BDE values and with the aid of computed radical reorganization energies (REs are close for CCSD(T)/CBS and B3LYP/B1 or B2 calculations), lead to barriers close to experiment and to high-level data. As such, the VB estimate of the barrier can be performed more or less from raw available data. Indeed, using the expression for D [Eq. (6)], the identity barrier for a HAT reaction can be written compactly as a balance of BDE and radical reorganization energy contributions [Eq. (11)].

$$\Delta E^{+}_{VB} = 0.1(\mathrm{BDE_{H\text{-}X}}) + 0.6|\mathrm{RE_{X\cdot}}| \quad (11)$$

Table 1 shows some interesting trends. Thus, H_2 and CH_4 (entries 1 and 2) have the same BDE, and nevertheless, CH_4 has a significantly higher identity barrier. Inspection of the data in these entries, shows that the difference in the corresponding barriers is brought about by the vertical bond strength D, which is larger for CH_3–H because of the significant reorganization energy of the $CH_3^{\cdot}$ radical (ca. 7 kcal mol^{-1}) compared with zero for H$^{\cdot}$. Thus, according to Equation (11), the radical reorganization energy (being part of D) accounts for the entire difference between these two reactions.

Another interesting comparison is the identity barriers for X = HCC and $NCCH_2$ (Table 1, entries 4 and 5, respectively). In this case, HCC–H has the higher BDE for the C–H bond, 37.2 kcal mol^{-1} higher, and nevertheless the reaction of $NCCH_2$–H ($NCCH_2^{\cdot} + NCCH_3 \rightarrow NCCH_3 + NCCH_2^{\cdot}$) has the higher barrier. The difference originates once more in the radical reorganization contribution to the vertical bond strength. Thus, the HCC$^{\cdot}$ radical is rigid and its reorganization term is negligible, whereas the $NCCH_2^{\cdot}$ radical, owing to its delocalization, has a reorganization energy of 10.8 kcal mol^{-1}, and this overrides the 3.7 kcal mol^{-1} contribution of the BDE term in Equation (11). Indeed, CH_3CN is notoriously sluggish in H-abstraction reactions.[59] Similarly, the high identity barrier for the benzyl radical (Table 1, entry 6)[56b] is due to the large reorganization energy of the radical (12 kcal mol^{-1}).

As seen from Equation (11), radicals pay an energetic price of 0.6 | $RE_{X\cdot}$ | during H-abstraction. Generally, monoatomic radicals (X$^{\cdot}$ = F$^{\cdot}$, H$^{\cdot}$) have zero reorganization energies

Table 1: BDE and D data (kcal mol^{-1}) and corresponding VB-derived barriers (kcal mol^{-1}) and experimental, CCSD(T)/CBS, and other calculated barriers for identity reactions, X$^{\cdot}$ + H–X → X–H + $^{\cdot}$X.

Entry	X	BDE[a]	D[a]	ΔE^{+}_{VB}[a]	$\Delta E^{+}_{CCSD(T)/CBS}$	ΔE^{+}_{exp}	ΔE^{+} (others)
1	H	103.2/104.2	103.2/104.2	10.3/10.4	8.8	9.7[b]	9.6[c]
2	CH_3	103.2/105.0	110.0/111.8	14.4/14.6	16.7	14.9[d]	17.8[c]
3	C_2H_5	96.9/101.4	103.9/108.4	13.9/14.3	–	–	14.3[e],16.7[c]
4	HCC	132.9/131.3	133.0/131.4	13.4/13.2	9.6	–	12.8[c]
5	$NCCH_2$	95.7/95.5	106.5/106.2	16.0/16.0	17.6	–	–
6	$PhCH_2$	85.8/89.8	98.1/102.3	15.9/16.4	–	19.9 ± 2.2[f] (18.7±2.2)	16.5[e]
7	F	135.1/136.3	135.1/136.3	13.5/13.6	13.9	–	–
8	OH	117.0/117.6	117.0/117.6	11.7/11.8	8.2	4.2[g]	[7.8](4.15) 7.3[h]
9	NH_2	105.3/106.7	105.4/106.7	10.6/10.7	11.0	–	–

[a] The BDE and D values are tabulated as calculated/experimental data, respectively. The calculated BDEs are at the CCSD(T)/CBS level in this work except entries 3 and 6 in which the B3LYP/B2 values were used from Ref. [39a]. The "experimental" D values were calculated using $D_{exp} = BDE_{exp} + RE_{calcd}$. The experimental BDE value for C_2H_5–H is taken from Ref. [58]. The experimental BDE value for $PhCH_2$–H is taken from Ref. [17d]. The VB predicted barriers are given as ΔE^{+}_{VB}(calcd)/ΔE^{+}_{VB}(exp) where the former uses calculated BDE and D data and the latter experimental data. [b] Taken from Ref. [56a]. [c] Classical barriers (V^{+} without ZPE correction) from data sets in Refs. [44]. [d] From Ref. [55]. [e] From Ref. [27a]. [f] Experimental E_a value from Ref. [56b]. In parentheses is a ΔH^{+} value estimated from E_a. [g] Experimental value taken from Ref. [56c]. [h] The value in square brackets is an activation barrier without ZPE-correction, the value in parentheses is the estimated activation barrier including the tunneling factor. The last value is the ZPE corrected barrier. Data from Ref. [57].

and radicals in which the spin density is localized on the abstracting atom (X$^{\bullet}$ = HO$^{\bullet}$, $H_2N^{\bullet}$, RO$^{\bullet}$, etc.) have very small reorganization energies. Alkyl radicals have reorganization energies of 7–9 kcal mol^{-1}, while highly stabilized and delocalized radicals have larger reorganization energies, approximately 12–20 kcal mol^{-1}. These radicals will pay an energetic price of 0.6 | $RE_{X^{\bullet}}$ | to "prepare" them for bonding. The entire set of BDE, *D*, and reorganization energies are collected in Tables S1, S5, S9, and S10 in the Supporting Information.

3.3. VB Modeling of Non-Identity HAT Barriers

The VB treatment of non-identity reactions, X$^{\bullet}$ + H-Y → X-H + $^{\bullet}$Y, requires two sets of BDE and *D* values. When the abstractor is a closed-shell molecule, an additional promotion energy quantity (ΔE_{ST}) that accounts for the cost of creating a radical at the abstractor site is required, as has been shown before,[35c] and as will be discussed further below (see Section 4.1 on closed-shell abstractors). All the requisite data including experimental barriers for 16 reactions are collected in the Supporting Information (Tables S11), while herein we discussed global behavior and a few specific cases.

Figure 3a shows the estimated VB barriers based on Equation (10a) and using experimentally based VB quantities (BDE, *D*), against experimental $\Delta G^{\neq}_{exp}$ at 298 K for 11 reactions (numbered according to Table S11). The reactant pairs X/H−Y are drawn in Figure 3 and it can be seen there are a few reactions with oxyl radical abstractors X$^{\bullet}$ (entries 1, 12–15 in Table S11), and others where the abstractor is a closed-shell molecule or ion, such as CrO_2Cl_2, MnO_4^-, and α-methylstyrene (entries 3–5, 7, 16, and 10 in Table S11). The correlation is seen to be reasonably good. An equally good correlation was obtained using $\Delta E^{\neq}_{VB}(1)$ based on theoretical values of the VB quantities, as shown in Figure 3b. It would have been perhaps more correct to correlate with the $\Delta H^{\neq}_{exp}$ data, but these data are scant (and perhaps somewhat less reliable than $\Delta G^{\neq}_{exp}$). The available six cases gave a correlation which is less good than with $\Delta G^{\neq}_{exp}$ though still tolerable, $R^2 = 0.786$ (Figure S5).

Generally speaking, the trends in the VB barriers in Figure 3 and in the entire set of 16 reactions we tested (Table S11) are similar to the experimental ones. A general observation from Figure 3 and the data in the Supporting Information is that the reactions in which the abstractor is an oxyl radical (reactions 1, 2, 12–15 in Figure 3) have smaller VB and experimental barriers compared with those reactions where the abstractor is closed-shell (3–5,7,10 and 16). Additionally, the numerical values of $\Delta E^{\neq}_{VB}$ are generally close to the available free energy barriers determined from experimental data. Let us describe some of the results and their insights into H-abstraction reactivity.

To initially demonstrate the facility of estimating barriers by usage of the VB model, let us take the flag reaction of $P450_{cam}$. In this reaction the active species Cpd I, having an oxyl radical in the FeO moiety, abstracts exclusively the *exo* C^5-H position of camphor, as depicted in Scheme 2.[2]

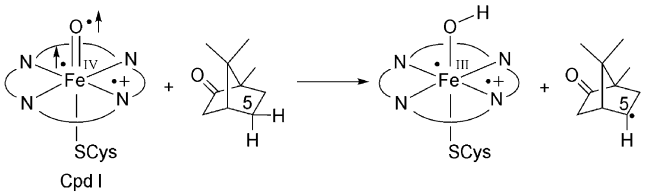

Scheme 2. The H-abstraction reaction of P450 Cpd I with camphor.

Using experimentally based BDE and *D* values, we get the following VB quantities: the average promotion energy G_0 is 212.2 kcal mol^{-1}, $\Delta E_{rp} = -1.7$ kcal mol^{-1}, and B = 48.6 kcal mol^{-1}. Using Equation (10), this leads to a VB predicted $\Delta E^{\neq}_{VB}(1)/\Delta E^{\neq}_{VB}(2)$ value of 14.2/14.2 kcal mol^{-1}. The use of B3LYP/B1-calculated BDE(*D*) values leads to a VB barrier of 15.5 kcal mol^{-1}, while the DFT computed barrier for the actual reaction is 15.2 kcal mol^{-1}.[39a,b] The kinetics of a single turnover lead to an experimental free energy barrier of $\Delta G^{\neq} \leq 15$ kcal mol^{-1},[60] while using the recent apparent rate constant, which is a product of the rate constant for the H-abstraction step and the equilibrium constant of camphor binding,[61a] and adding the camphor binding free energy[61b,c] can give an upper limit for the barrier of 17 kcal mol^{-1}. All in all, the VB model makes a reasonable prediction of the barrier for the flag reaction of P450 enzymes.

Let us turn now to Figure 3 to compare barriers for different abstractors reacting with the same H−Y molecules. Thus, comparisons of reactions of *t*BuO$^{\bullet}$ and *t*BuOO$^{\bullet}$ with

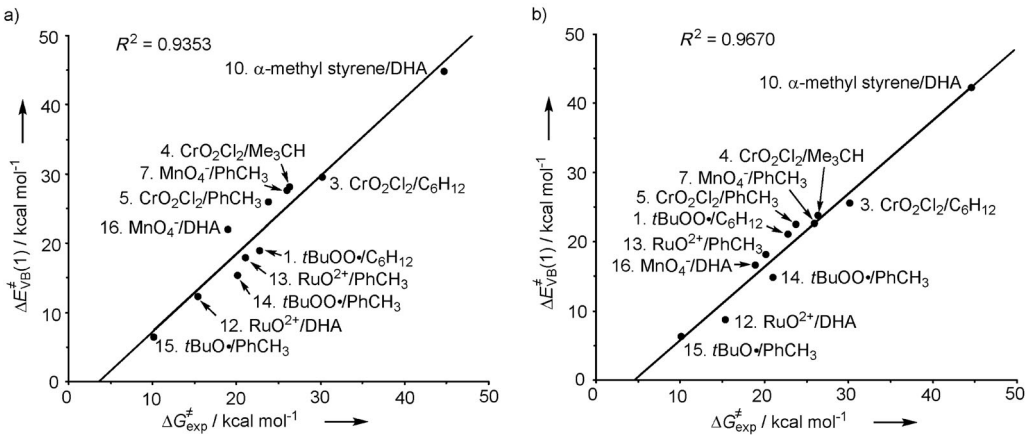

Figure 3. Plots of $\Delta E^{\neq}_{VB}(1)$ vs $\Delta G^{\neq}_{exp}$ at for X$^{\bullet}$ + H-Y → X-H + $^{\bullet}$Y non-identity reactions. The VB barriers are calculated, a) using experimentally based BDE and *D* values, and b) B3LYP/B1 BDE and *D* values. The reactants and reaction numbers are the same as the entry numbers in Table S11 of the Supporting Information.

the same alkane, for example, reactions 14 and 15 show that *t*BuOO• has a much higher barrier than the corresponding reaction with *t*BuO•.[17b,28a,62] Using the corresponding *D* and BDE values (Supporting Information Tables S9–S10), it can be further concluded that the VB-predicted intrinsic barriers [Eq. (10c)] are somewhat similar for the two abstractors. As such, it can be concluded that the relative barriers are primarily determined by the corresponding thermodynamic driving forces, rendering the more exothermic reactions of *t*BuO• much faster than those of *t*BuOO•, in accord with the BEP principle.[30]

Let us now compare reactions 1, in which the abstractor is *t*BuOO•, to 3 where the abstractor is CrO_2Cl_2, and in both reactions the H–Y molecule is cyclohexane (C_6H_{12}, Figure 3).[17b] Even though CrO_2Cl_2 has the option to react with alkanes by a 3+2 cycloaddition reaction, which occurs for OsO_4 and other metal oxides with alkenes,[63] and for MnO_4^- with H_2,[64] Mayer has shown convincingly that the Ètard reaction (reaction 3) proceeds by H-abstraction, and Limberg[19] has supported the Mayer mechanism. Therefore we treated both reactions as H-abstractions. It is seen from Figure 3 that the predicted VB barriers reproduce the experimental trends, and the barrier of reaction 3 is about 9 kcal mol^{-1} higher than that of reaction 1, where the abstractor is the radical *t*BuOO•. Using experimental bond dissociation free energies (BDFEs),[28d,65] the two reactions have virtually the same driving force, while the use of experimental BDEs (i.e., enthalpies),[28b] shows that the reaction *t*BuOO• + C_6H_{12} is less endothermic than that for $CrO_2Cl_2 + C_6H_{12}$, but not sufficiently so to account for the barrier difference. Thus, in any event, the thermodynamic driving force alone cannot account for the difference in the barriers, $\Delta H^{\neq}(\Delta G^{\neq}) = 26.6$ (30.2) kcal mol^{-1} (reaction 3) and $\Delta H^{\neq}(\Delta G^{\neq}) = 18.9$ (22.8) kcal mol^{-1} (reaction 1).[17b] The root cause of this difference must then be the higher intrinsic barrier of reaction 3. Similar considerations seem to be applicable to the comparison of reaction 7 of the closed-shell MnO_4^- with $PhCH_3$[17c,e] to reaction 14 of *t*BuOO• with the same substrate (Figure 3). Another reaction of a closed-shell abstractor is the Rüchardt reaction (reaction 10, Figure 3)[18] wherein the abstractor is α-methylstyrene reacting with DHA and resulting in the highest barrier in the series ($\Delta G^{\neq} \approx 44.7$ kcal mol^{-1}). Comparison with the analogous reaction of cumyl radical with DHA (entry 11, Table S11) would reveal again that the predicted VB barriers show correctly a huge advantage of the reaction with the radical abstractor. Still however, there are closed-shell abstractors, which react fast. For example, the H-abstraction reactions by ketones from ketyl radicals[20] have free energy barriers of the order of 12 kcal mol^{-1}, and the identity free energy barrier in the reaction of CrO_2Cl_2 with $CrOCl_2(OH)$• was estimated to be only 12.9 kcal mol^{-1} from the reaction of the CrO_2Cl_2 abstractor with toluene,[28b] and so on.

The questions which we need to address now are: 1) what is the difference between the closed-shell and open-shell H-abstractors from the VB perspective? 2) Why do some abstractors have quite high HAT reactivity despite their closed-shell nature? To answer these questions, we first have to derive the intrinsic barriers and their component identity barriers, and subsequently try to predict these quantities from raw data using the VB model.

3.4. VB Modeling of Intrinsic Barriers and Their Identity Components Derived from The Marcus Equation

Given the free energy barrier and the driving force of a reaction, the Marcus Equations (3a) and (3b) allow extraction of "experimental" intrinsic and identity barriers. In principle this is easy, but it must be remembered that the value of the intrinsic barrier so extracted is very sensitive to the value of the driving force used in the equation. Different values of BDE and BDFE[65] (or the presence/absence of different cluster energies, e.g., owing to hydrogen bonding and the resulting solvent effects), can generate intrinsic barriers that differ by quite a few kcal mol^{-1} (at least half of the difference in the driving force obtained using different data; see Equation (3a)]. Therefore, instead of presenting an exhaustive list of intrinsic barrier values, we focus herein on only a few reactions where the conclusions have clear mechanistic significance. The rest of the data is summarized in the Supporting Information, Tables S11 and S12, which list experimental intrinsic and identity barriers along with VB estimates.

Table 2 shows these quantities for three reactions, *t*BuOO• and CrO_2Cl_2 reacting with cyclohexane (C_6H_{12}), and the reaction of CrO_2Cl_2 with $PhCH_3$. Using the driving-force values, $\Delta H_{rp}(\Delta G_{rp})$, along with the experimental enthalpies and free energies of activation, $\Delta H^{\neq}(\Delta G^{\neq})$, we obtain, from the Marcus equation, the corresponding intrinsic barriers,

Table 2: Experimental barriers, driving forces, intrinsic and identity barriers (kcal mol^{-1}) for some X + H–Y → X–H + Y reactions, involving one radical and one closed-shell abstractor.

	X/H–Y	$\Delta H^{\neq}[\Delta G^{\neq}]$[a]	$\Delta H_{rp}[\Delta G_{rp}]$[c]	$\Delta H^{\neq}_0[\Delta G^{\neq}_0]$[d]	$\Delta H^{\neq}_{XX}[\Delta G^{\neq}_{XX}]$[d]	$\Delta H^{\neq}_{YY}(\Delta G^{\neq}_{YY})$
1	*t*BuOO•/C_6H_{12}	18.9 (22.8)[b]	10.3 (10.7)	13.2 (17.0)	12.7 (13.8)[b]	13.8 (20.2)
2	CrO_2Cl_2/C_6H_{12}	26.6 (30.2)	16.3 (10.4)	17.5 (25.1)	21.2 (30.0)	13.8 (20.2)
3	$CrO_2Cl_2/PhCH_3$	15.5 (23.8)	6.9 (6.3)	11.8 (20.9)	4.9(18.4)(12.9[e])	18.7 (23.4)

[a] Data from Ref. [17b], scaled to reactivity for one H and to $T = 298$ K. [b] The data for this reaction is from Ref. [66]. The $\Delta H^{\neq}_{XX}$ value using the activation energy and hydrogen-bonding association is 10.5 kcal mol^{-1}. Since tunneling seems to be involved, $\Delta H^{\neq}_{XX} > 10.5$ kcal mol^{-1}. A value of approximately 12 kcal mol^{-1} appears in Ref. [6a]. The above tabulated $\Delta H^{\neq}_{XX}$ value leads to a good estimate of $\Delta H^{\neq}_{YY}$ and is hence used. [c] BDE and BDFE data from Tables S9 and S10 in the Supporting Information. [d] $\Delta H^{\neq}_0(\Delta G^{\neq}_0)$ are extracted from the experimental $\Delta H^{\neq}(\Delta G^{\neq})$ data using Equation (3a), $\Delta H^{\neq}_{XX}(\Delta G^{\neq}_{XX})$ values are extracted from the intrinsic barriers and Equation (3b). [e] An estimated experimental free energy barrier value from the rate constant in Ref. [28b].

$\Delta H^{\neq}_0(\Delta G^{\neq}_0)$. Comparison of the first two reactions shows that both the enthalpic and free energetic intrinsic barriers are significantly larger for the closed-shell abstractor CrO_2Cl_2. Since both reactions proceed with the same cycloalkane, C_6H_{12}, then the difference in the intrinsic barriers means that the identity barrier for $CrO_2Cl_2/CrOCl_2(OH)^{\bullet}$ should be larger than that of *t*BuOO$^{\bullet}$/*t*BuOOH. The corresponding identity barriers are extracted from Equation (3b) in the following manner: using the reported identity rate constant for *t*BuOO$^{\bullet}$/*t*BuOOH[17b,66] leads the corresponding identity free energy barrier, which in turn is used to gauge the barriers for $C_6H_{11}^{\bullet}/C_6H_{12}$, 13.8 (20.2) kcal mol^{-1}, which are reasonable for simple alkyl/alkane combinations (e.g., $CH_3^{\bullet}/CH_4$[55a] and $PhCH_2^{\bullet}/PhCH_3$[56b] in Table 1). These $C_6H_{11}^{\bullet}/C_6H_{12}$ barrier values, in turn, allow the identity barriers for $CrO_2Cl_2/CrOCl_2(OH)^{\bullet}$ to be estimated. It is seen that these barriers are $\Delta H^{\neq}_{XX}(\Delta G^{\neq}_{XX}) = 21.2$ (30.0) kcal mol^{-1}, namely, 8.5 (16.2) kcal mol^{-1} higher than the values for the open-shell abstractor *t*BuOO$^{\bullet}$.

Now, considering the reaction of CrO_2Cl_2 with toluene (Table 2, entry 3) we encounter some surprises. Firstly, the corresponding intrinsic barriers, $\Delta H^{\neq}_0(\Delta G^{\neq}_0) = 11.8$ (20.9) kcal mol^{-1}, are 4–6 kcal mol^{-1} smaller than for the reaction with cyclohexane. Moreover, after using the known identity barrier for $PhCH_2^{\bullet}/PhCH_3$, $\Delta H^{\neq}_{YY}(\Delta G^{\neq}_{YY}) = 18.7$ (23.4) kcal mol^{-1},[56b] the identity barriers so derived for $CrO_2Cl_2/CrOCl_2(OH)^{\bullet}$ are $\Delta H^{\neq}_{XX}(\Delta G^{\neq}_{XX}) = 4.9$ (18.4) kcal mol^{-1}, certainly much smaller than those determined from the reaction of CrO_2Cl_2 with cyclohexane, by 12–16 kcal mol^{-1}. An experimental estimate of this identity free energy barrier (using the reaction with toluene) was also reported[28b] to be 12.9 kcal mol^{-1} (the origins of the 5.5 kcal mol^{-1} disparity in the $\Delta G^{\neq}_{XX}$ value compared to ours is not clear). Any of these values is much smaller than the corresponding values extracted from the reaction of CrO_2Cl_2 with cyclohexane. It is very clear in this case that the experimental data for two related reactions (Table 2, entries 2 and 3) lead to very different identity barriers for $CrO_2Cl_2/CrOCl_2(OH)^{\bullet}$. As shall be seen, this intriguing finding is not accidental.

A similar dichotomy seems to exist in the reactions of MnO_4^- with hydrocarbons. A Marcus analysis of the B3LYP/B1 barriers[67] for reactions of MnO_4^- and *t*BuOO$^{\bullet}$ with CH_4 leads to $\Delta H^{\neq}_{XX} = 21.6$ kcal mol^{-1} for $MnO_4^-/MnO_3(OH)^{\bullet-}$, much larger than the corresponding value of 7.1 kcal mol^{-1} for *t*BuOO$^{\bullet}$/*t*BuOOH (for both reactions, we use a B3LYP/B1 identity barrier of 14.6 kcal mol^{-1} for $CH_3^{\bullet}/CH_4$). Moving on to alkanes with weaker C–H bonds yields smaller identity-barrier values. Thus, using the experimental barriers for the reaction of MnO_4^- with $PhCH_3$ $\Delta H^{\neq}(\Delta G^{\neq}) = 20.0$ (26.0) kcal mol^{-1},[17e] along with the values for the driving force, $\Delta H_{rp}(\Delta G_{rp}) = 9.9$ (6.3) kcal mol^{-1}, lead to the following intrinsic barriers, $\Delta H^{\neq}_0(\Delta G^{\neq}_0) = 14.6$ (22.7) kcal mol^{-1}, which yield in turn, identity barriers of $\Delta H^{\neq}_{XX}(\Delta G^{\neq}_{XX}) = 10.6$ (22.1) kcal mol^{-1} for $MnO_4^-/MnO_3(OH)^{\bullet-}$. In the reaction of MnO_4^- with DHA (using the values $\Delta H^{\neq}_{exp}(\Delta G^{\neq}_{exp}) = 13.9$ (19.0) kcal mol^{-1} and $\Delta H_{rp}(\Delta G_{rp}) = -2.0$ (-5.7) kcal mol^{-1}), application of the Marcus equation leads to $\Delta H^{\neq}_0(\Delta G^{\neq}_0) =$ 14.9 (21.8) kcal mol^{-1}. Using the reported Marcus analysis based value of the rate constant,[17e] 5×10^{-11} M^{-1}s^{-1}, for the identity reaction DHA(-H$^{\bullet}$)/DHA,[28d,e,68] yields an identity free energy barrier of 31.5 kcal mol^{-1}. Using this value and the intrinsic free energy barrier, $\Delta G^{\neq}_0 = 21.8$ kcal mol^{-1}, in Equation (3b), leads to an identity free energy barrier of $\Delta G^{\neq}(MnO_4^-/MnO_3(OH)^{\bullet-}) = 12.1$ kcal mol^{-1} for $MnO_4^-/MnO_3(OH)^{\bullet-}$. In contrast, our own B3LYP/B1 calculations for DHA(-H$^{\bullet}$)/DHA find a ZPE corrected barrier of 17.2 kcal mol^{-1}, and the VB model predicts a matching value, $\Delta E^{\neq}_{VB}(DHA(-H^{\bullet})/DHA) = 16.5$ kcal mol^{-1}. Based on the free energy barrier of the analogous identity reaction $\Delta G^{\neq}(PhCH_2^{\bullet}/PhCH_3) = 23.4$ kcal mol^{-1}, a free energy barrier of 23–24 kcal mol^{-1} for DHA(-H$^{\bullet}$)/DHA seems more realistic than the very high value of 31.5 kcal mol^{-1}.[28d,e,68] Using this lower DHA(-H$^{\bullet}$)/DHA barrier, would lead to $\Delta G^{\neq}(MnO_4^-/MnO_3(OH)^{\bullet-}) \approx 19.6$–20.6 kcal mol^{-1}. To get an enthalpic identity barrier, we used the B3LYP/B1 barrier $\Delta H^{\neq}(DHA(-H^{\bullet})/DHA) = 17.2$ kcal mol^{-1}, which leads to $\Delta H^{\neq}(MnO_4^-/MnO_3(OH)^{\bullet-}) = 12.6$ kcal mol^{-1}. It is clear that these identity barriers are smaller than the one determined above for $MnO_4^-/MnO_3(OH)^{\bullet-}$ from the reaction of MnO_4^- with CH_4, and certainly much smaller than the value for $CrO_2Cl_2/CrOCl_2(OH)^{\bullet}$, extracted from the reaction of CrO_2Cl_2 with C_6H_{12} (Table 2), but of the same magnitude as the $CrO_2Cl_2/CrOCl_2(OH)^{\bullet}$ barrier extracted from the reaction of CrO_2Cl_2 with $PhCH_3$. Thus, we can see again that closed-shell abstractors have in some cases large self H-exchange barriers compared with their open-shell oxyl radical abstractors, while in other cases the self H-exchange barriers are small and about the same as for the open-shell cases. This dichotomy merits understanding.

4. The Dichotomy of Closed-Shell H-Abstractors

According to the VB model, a closed-shell abstractor may abstract a hydrogen atom, but in so doing it must eventually undergo additional reorganization to create a radical species at the site of abstraction. This reorganization is dictated by the electronic structure of the product state, as was shown more than a decade ago[35c] for the Ètard reaction. If this reorganization is the entire difference compared to a radical abstractor, then this will necessarily mean that the promotion gap in the VB diagram that describes the reaction for the closed-shell abstractor will be larger than for a reaction of a radical species with the same substrate. The higher promotion energy reflects the cost of creating unpaired electron density at the abstractor center and its size gauges the intrinsic barrier. Therefore, in principle, closed-shell abstractors will have sluggish H-abstraction reactivity. However, since some reactions of closed-shell abstractors are seen above to be quite fast, it follows that closed-shell abstractors must have also alternative mechanisms whereby in some cases, they can abstract a hydrogen atom, *while evading paying the cost of this additional promotion energy*. This Section addresses the dichotomic reactivity of closed-shell abstractors.

4.1. The Promotion-Energy Contribution to High Barriers in H-Abstractions by Closed-Shell Molecules

Figure 4 a,b shows the H-abstraction reactivity of CrO_2Cl_2 and *t*BuOO• towards the same alkane, H–Y,[35c] assuming both reactions follow the normal HAT hydrogen-atom abstraction mechanism. Since CrO_2Cl_2 is a closed-shell molecule with two Cr=O double bonds, the only way to eventually make the new O–H bond and create a Cr• radical is to uncouple the Cr=O bond into a triplet as shown in Figure 4 a. Thus in the promoted state the triplet •Cr–O• and H••Y are paired such that the oxyl radical of •Cr–O• pairs with the H• species to form a new bond pair and a singlet diradical (one electron on the Cr• center which has d^1 configuration and the other on Y•).[69] In contrast, in Figure 4 b, in which the initial abstractor is already a radical, the promotion energy at the reactant side involves only the H–Y bond.

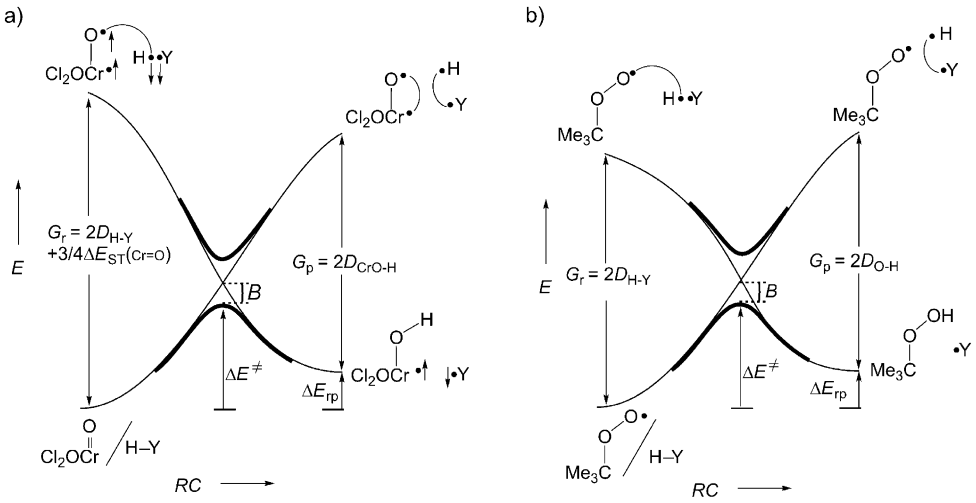

Figure 4. VBSCDs for the reactions of two oxidants reacting with an alkane H–Y in the normal HAT mechanism. a) The oxidant is CrO_2Cl_2, and b) the oxidant is *t*BuOO•.

It is very clear that with this description, the barrier for the closed-shell abstractor will be raised in proportion to this additional promotion energy, which for the present example is $\Delta E_{ST}(CrO_2Cl_2)$. If we therefore compare two reactions wherein, except for G_r, all the other VBSCD parameters (Figure 4 a,b) are identical, then the difference in the two barriers will derive solely from the value of the additional singlet–triplet excitation required to convert the closed-shell CrO_2Cl_2 into a •Cr–O• diradical.

For the specific comparison of the two abstractors, *t*BuOO• and CrO_2Cl_2, reacting with C_6H_{12}, the only VB quantity that changes significantly is the promotion energy G_r, while the B and G_p are almost the same for the two reactions (Supporting Information, Table S11). Hence, using Equation (10), the VB-predicted barrier difference for the two reactions can be written as in Equation (12).

$$\Delta E^{\neq}{}_{VB}(CrO_2Cl_2) - \Delta E^{\neq}{}_{VB}(t\text{BuOO}^{\bullet}) \approx (3/8)\, f_0\, \Delta E_{ST}(CrO_2Cl_2) \quad (12)$$

Using the experimental data for CrO_2Cl_2,[70] the lowest triplet state is 55.3 kcal mol^{-1} above the ground state. Our own theoretical calculations show that the values of the singlet–triplet promotion are 45.4 kcal mol^{-1} (B3LYP/Def2-TZVP//Def2-TZVP, see Supporting Information, Table S9) and 40.1 kcal mol^{-1} (LACV3P + */LACVP*, see Table S9). Plugging the $\Delta E_{ST}(CrO_2Cl_2)$ values into Equation (12), yields an energy barrier differences of $\Delta\Delta E^{\neq}{}_{VB}(CrO_2Cl_2$–*t*BuOO•) = 4.5–6.2 kcal mol^{-1} versus 7.7 (7.4) kcal mol^{-1} barrier difference derived from experiment (Table 2). Furthermore, the VB model predicts that this will also be the difference in the corresponding intrinsic barriers. Inspection of Table 2 shows that difference of the experimentally based intrinsic barriers are indeed $\Delta\Delta H^{\neq}{}_0(\Delta\Delta G^{\neq}{}_0) = 4.3$ (8.1) kcal mol^{-1}.

The identity barrier for the self H-exchange reaction, $CrO_2Cl_2/CrOCl_2(OH)$• can also be compared to the corresponding one for the oxyl radical *t*BuOO•. In this case, the barrier difference is doubled, because the promotion gap G_r is not averaged as in the expression for the intrinsic barrier, thus leading to Equation (13).

$$\Delta E^{\neq}{}_{VB,XX}(CrO_2Cl_2/CrOCl_2(OH)^{\bullet}) - \Delta E^{\neq}{}_{VB,XX}(t\text{BuOO}^{\bullet}/t\text{BuOOH}) \approx (3/4)\, f_0\, \Delta E_{ST}(CrO_2Cl_2) \quad (13)$$

Using the values above, we predict 9.0–12.4 kcal mol^{-1} of excess identity barrier for the closed-shell abstractor, compared with 8.5 (16.2) kcal mol^{-1} derived from experimental enthalpies (free energies) of activation in Table 2 (entry 2). Another interesting result is the high identity barrier measured and computed for the self H-exchange of vanadium(V) dioxo/vanadium(IV) oxo hydroxo systems compared with the analogous reaction of the structurally related open-shell abstractor ruthenium(IV) oxo/ruthenium(III) hydroxo. The experimental rate constant of the vanadium system is six orders of magnitude lower than the ruthenium system (a difference of 8.4 kcal mol^{-1} in free energies), and the corresponding barrier is calculated to be approximately 6 kcal mol^{-1} higher.[25] Using Equation (13) with the B3LYP/B1 computed $\Delta E_{ST}(VO_2) = 57$ kcal mol^{-1} the VB model predicts a difference of 12.8 kcal mol^{-1} in the barrier relative to an open-shell system in which all other parameters, except for the extra promotion energy, are almost the same.

In the general case, Equation (14) should be used to predict the barrier differences, as an interplay of the contribution arising from the "penalty" of singlet–triplet promotion of the closed-shell molecule, and the increment owing to the reaction-driving forces, which tend also to make

the H-abstraction by closed-shell molecules less exothermic or more endothermic than its open-shell congener, and lastly also, the difference in the transition-state resonance energies.

$$\Delta E^{\neq}_{VB}(\text{closed-shell X}) - \Delta E^{\neq}_{VB}(\text{open-shell X}^{\bullet}) \approx (3/8)\, f_0\, \Delta E_{ST}(\text{closed-shell X}) + {}^1/_2\, \Delta\Delta E_{rp} + \Delta B \quad (14)$$

4.2. Why Some H-abstraction Reactions by Closed-Shell Molecules are Nevertheless Fast?

The above examples follow the data in Figure 4a rather well. Still, this does not explain the puzzling dichotomy, noted in Table 2 and in the follow-up discussion, of different identity barriers estimated for the same self H-exchange reaction from different non-identity reactions. Thus, from Table 2, it would seem that closed-shell reagents could participate in H-abstractions in two distinct manners. In one manner, for example, CrO_2Cl_2 abstracting H from cyclohexane, the reagent has to pay the penalty of the extra promotion energy required to create a radical at the abstractor center. However, in the alternative manner, for example, CrO_2Cl_2 with $PhCH_3$ (Table 2), or MnO_4^- with DHA, the closed-shell abstractors somehow manage to avoid this penalty. In fact, using the VB model with the promotion-gap expression as in Figure 4a, predicts very well the $CrO_2Cl_2/CrCl_2(OH)^{\bullet}$ barrier from the reaction of CrO_2Cl_2 with C_6H_{12}, but would *overestimate* the corresponding reaction barriers and the identity barriers for the reactions of CrO_2Cl_2 with $PhCH_3$ and MnO_4^- with $PhCH_3$ or DHA. However, if we arbitrarily delete the ΔE_{ST} term from the promotion gap expression, the predicted barrier for the reaction of CrO_2Cl_2 with toluene will be only 16–17.4 kcal mol^{-1}, in good agreement with $\Delta H^{\neq}_{exp} =$ 15.5 kcal mol^{-1} (Table 2). In this case, the identity barrier for the self H-exchange reaction $CrO_2Cl_2/CrOCl_2(OH)^{\bullet}$ would also be low and close to the experimental data estimated from the reaction with toluene (12.9 kcal mol^{-1}, Table 2). Similarly, ignoring the singlet–triplet promotion term for MnO_4^- will lead to intrinsic and identity barriers much closer to the experimental data.[28b] But how could MnO_4^- and CrO_2Cl_2 evade the need for this promotion, in some of their reactions, if this is needed to create the product ground state (Figure 4a)?

4.2.1. The Proton-Coupled Electron Transfer (PCET) Option for H-Abstraction

The answer to the above question lies in the PCET mechanism, or more generally, in mechanisms in which the transition states have blended hydrogen-atom transfer (HAT) and proton transfer (PT), or hydride transfer (HT) characters. Thus, to tie off the loose ends, let us first analyze the HAT versus PCET mechanistic options for abstracting a hydrogen atom.

First we consider these options for a reaction of an X$^{\bullet}$ radical with an H–Y molecule. As has been nicely demonstrated by Mayer and Borden,[27] using B3LYP computations, when the H-abstractor is an alkoxy radical and the H–Y molecule has an O–H bond (e.g., an alcohol), there are two alternative ways to transfer the H atom, which are depicted in Scheme 3a,b.

Scheme 3a describes a standard HAT, in which the O-H-O moiety in the transition state involves three electrons, one contributed by the alkoxyl radical center and two by the

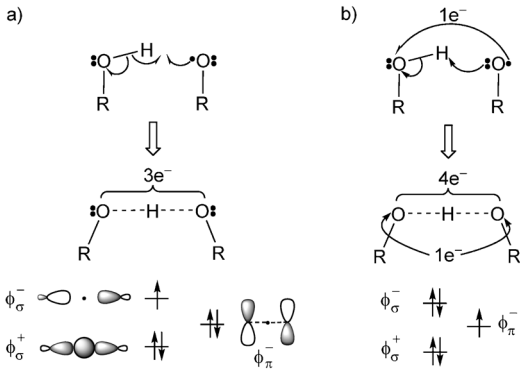

Scheme 3. Alkoxy-radical/alcohol pairs can participate in: a) a HAT process, and b) a PCET process.

H–O bond pair, giving a 3-electron/3-center transition state. The characteristic orbitals of such a transition state are the doubly occupied bonding orbital along the O-H-O axis, ϕ_σ^+, and the singly occupied nonbonding-type orbital, ϕ_σ^-, which has a node on the H atom in transit. Scheme 3a shows also the orbital ϕ_π^- which is perpendicular to the O-H-O axis. ϕ_π^- corresponds to the negative combination of the two 2p lone-pairs on the oxygen moieties, and will involve delocalization into the R moieties, which in turn will influence its relative energy to ϕ_σ^-. Scheme 3b describes the alternative mechanism whereby the electron pair on the alkoxyl radical abstracts a proton from the H–O bond, such that the O-H-O moiety of the transition state involves four electrons, while the unpaired electron, initially on the right-hand alkoxyl center, is now delocalized over the right- and left-side oxygen moieties. In the orbital occupation scheme, the axis orbitals are now both doubly filled, while the odd electron occupies the ϕ_π^- orbital, perpendicular to the O-H-O axis. This latter option is a concerted PCET, in which the proton is transferred along one axis and the electron is transferred between orbitals perpendicular to this axis, such that the net effect is a hydrogen-atom transfer.

One advantage of the PCET mechanism is the rather low energy of the 4-electron/3-center proton-abstraction transition states wherein the proton can be highly stabilized by the two negatively charged O moieties that flank the positively charged H. In the VB language, the 4-electron/3-center transition state of proton transfer reactions have a significant character of the triple ionic structure, $O:^- H^+ {}^-:O$.[35c,48,71] Such a 4-electron/3-center transition state requires that both groups that flank the proton will be electronegative and be able to sustain a negative charge. Indeed, PCET transition states were located only for alkoxy/alcohol pairs, while alkyl radical/alkane combinations, such as $PhCH_2^{\bullet}/PhCH_3$, proceed by the normal HAT option. Moreover, it was shown[27] that in

a given O-H-O arrangement, the HAT and PCET states coexist, and the lowest state depends on the identity of the alkoxy/alcohol pair. Thus, for $CH_3O^{\bullet}/CH_3OH$ the HAT transition state is more stable by approximately 5–6 kcal mol^{-1}, while for $PhO^{\bullet}$/PhOH, the PCET transition state is lower by about 6 kcal mol^{-1}, which is in accord with the higher electron affinity (EA) of $PhO^{\bullet}$ compared with $CH_3O^{\bullet}$.[72,73]

4.2.2. *Hybrid HAT–PCET Nature in H-Abstraction by Closed-Shell Abstractors*

Before VB modeling of PCET is attempted, we have to make a case for the existence of PCET and the PCET/HAT mechanistic dichotomy, in the reactions of the closed-shell abstractors discussed above in Figure 3 and Table 2. Consider for example, the identity reaction of MnO_4^- with $MnO_3(OH)^{\bullet-}$, which may proceed by two different mechanisms as simplified in Scheme 4. In this case MnO_4^- is the closed-shell abstractor in which the Mn center has no d electrons (d^0), whereas in $MnO_3(OH)^{\bullet-}$, the Mn center is d^1 with one electron in a d-type orbital on Mn. Scheme 4a shows the "normal" HAT in which three electrons are delocalized over the O-H-O moiety, and the electrons of the Mn=O bond (Scheme 4a, right) are unpaired to create the oxyl radical center and the Mn(d^1) center. In this case, as discussed above in Scheme 3a, we would expect to find an unpaired electron in the ϕ_σ^- orbital along the O-H-O axis.

Scheme 4b shows the alternative PCET. In this case the oxygen lone pair of the Mn=O moiety acts as a base and abstracts a proton from $MnO_3(OH)^{\bullet-}$, while at the same time, the unpaired electron, initially at the d-type orbital of the left-hand side Mn center, undergoes delocalization to the right-hand side Mn. As such, we would expect to see a singly occupied ϕ_d^+ orbital off the O-H-O axis. The same dichotomy applies of course to the identity reaction of $CrO_2Cl_2/CrOCl_2(OH)^{\bullet}$.

Since the PCET mechanism should have a highly stabilized charge-alternated $O^{\delta-}$-$H^{\delta+}$-$O^{\delta-}$ transition-state moiety, with the unpaired electron stored in the low-lying Mn d-orbitals, we might expect that PCET will be preferred over the normal HAT mechanism that requires paying the penalty of triplet decoupling of the π(Mn=O) bond. However, in the non-identity reaction with some alkanes, HAT will be preferred over PCET. To test this hypothesis and additionally demonstrate the dichotomy of the closed-shell abstractors we present herein our own B3LYP/B1 calculations of the identity reaction, of MnO_4^- with $MnO_3(OH)^{\bullet-}$, and the reaction of MnO_4^- with C_6H_{12}.

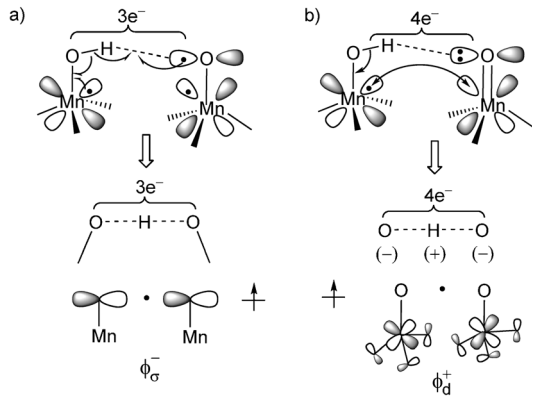

Scheme 4. Electron reorganization during a) HAT, and b) PCET in the identity reaction of MnO_4^- with $MnO_3(OH)^{\bullet-}$. Underneath the structures, the expected singly occupied orbitals are shown.

Figure 5 shows the transition states for the two reactions. As seen in Figure 5a, in the self H-exchange reaction, the unpaired electron is in a ϕ_d^+ type natural orbital (NO) that is composed of the two d_δ orbitals on the Mn atoms, and is not involved in the O-H-O axis, as envisioned in Scheme 4b. It is further seen that the O-H-O moiety has very little spin distribution (−0.17), but a strong triple ionic character with alternating charges ($Q_{O\text{-}H\text{-}O} = -0.72, +0.49, -0.72$). These features characterize a PCET as discussed in light of Scheme 4b. It is seen that the computed identity barrier for this reaction is 11.9 kcal mol^{-1}, comparable to the estimated

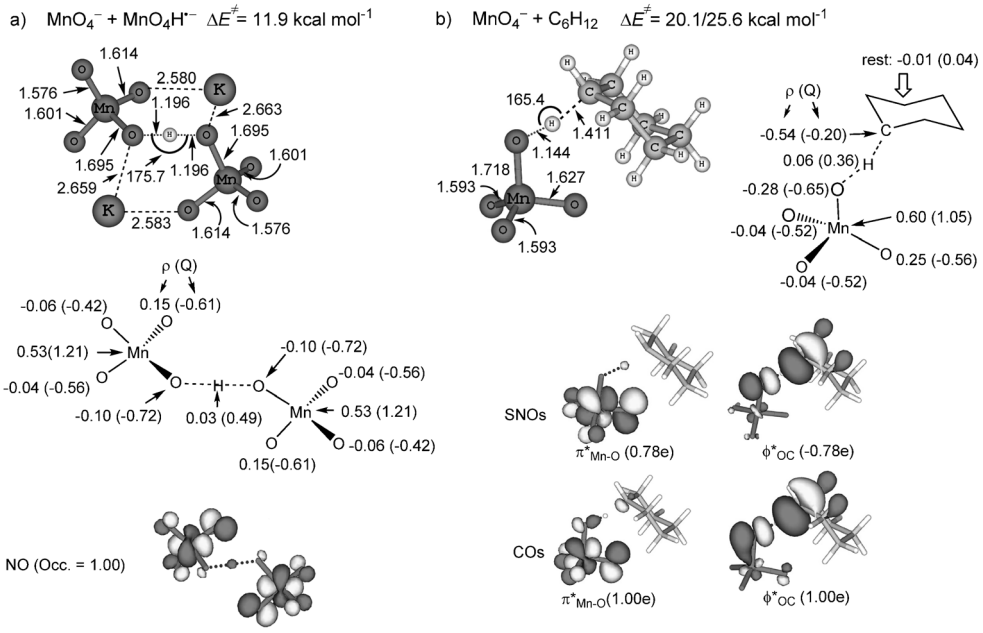

Figure 5. B3LYP/B1 data: Barriers, structures, spin (ρ) and charge (Q) distributions, and spin natural orbitals (SNOs) and corresponding orbitals (COs) for, a) the transition state for the identity H-abstraction of MnO_4^- with $MnO_3(OH)^{\bullet-}$, and b) the non-identity H-abstraction of MnO_4^- with C_6H_{12} (the barriers of the non-identity H-abstraction of MnO_4^- with C_6H_{12} correspond to open-shell/closed-shell transition states).

value $\Delta H^{\neq}(MnO_4^-/MnO_3(OH)^{\bullet-}) = 10.6$ kcal mol^{-1} from the Marcus equation applied to the reaction of MnO_4^- with $PhCH_3$ (see Section 3.4).

In contrast to the identity reaction, we see a different transition-state type for the reaction of MnO_4^- with C_6H_{12} in Figure 5b. Now the O-H-C moiety involves significant spin density of −0.76, as would be expected for a normal HAT transition state. Furthermore, considering the spin natural orbitals (SNOs) of the open-shell transition state, reveals that the spin distribution corresponds to one spin-up electron on the Mn center, and one spin-down electron in a ϕ_σ^- orbital that lies on the O-H-C axis and has a node on the H atom, as would be expected from a 3-electron/3-center HAT transition state exemplified in Scheme 3a. Additionally, the natural orbitals (NOs) of this open-shell transition state can be transformed to corresponding-orbitals (COs). This transformation in a way removes the effect of spin-symmetry breakage in DFT and produces two COs, each with 1e occupancy, and akin to generalized valence bond orbitals. These COs are seen to be almost identical to the SNOs, one on Mn while the other is in a ϕ_σ^- C-H-O orbital having a node on the H moiety, thus characterizing a standard HAT process. The ZPE-corrected B3LYP/B1 barrier is 20.1/25.6 kcal mol^{-1} relative to the cluster of the two reactants. Using the VB quantities computed at the same B3LYP/B1 level (Supporting Information, Table S12), the VB model, which includes the $\Delta E_{ST}(MnO_4^-)$ promotion energy penalty as in Figure 4a, predicts VB barrier $\Delta E^{\neq}_{VB}(1)/\Delta E^{\neq}_{VB}(2) = 25.7/26.0$ kcal mol^{-1}, which is close to the B3LYP results of 20.1/25.6 kcal mol^{-1}.

The above results support our VB analysis that the reactions of CrO_2Cl_2 and MnO_4^- (and other closed-shell abstractors) with alkanes will exhibit a dichotomous identity reaction that will depend on the alkane. In a case, such as cyclohexane, which is not too capable of stabilizing a negative charge on the carbon moiety, the closed-shell abstractors MnO_4^- and CrO_2Cl_2 will pay the penalty of decoupling the electrons of metal oxo π-bond needed for participating in a normal HAT transition state (Figure 4a), and will thus have a high identity barrier contribution to the corresponding intrinsic barrier. In contrast, in the case of the reactions of CrO_2Cl_2 or MnO_4^- with an alkane which has a very weak C–H bond, the abstractor may use its PCET option, and since the PCET and HAT characters are not really orthogonal in these reactions it is anticipated that the transition states will involve generally a variable mixture of PCET and HAT depending on the alkane.

5. VB Modeling of Hybrid HAT and PCET Reactivity in H-Abstraction

5.1. VB Models for HAT and PCET in H-Abstraction by Radicals

While the above computational results make a clear case for a hybrid PCET/HAT reactivity for the closed-shell MnO_4^- abstractor, we still have to present a VB model that will allow bridging between the classical HAT model in Figure 4 and the PCET mechanism.

The easiest way to introduce this dichotomy is to start by analyzing the well-studied reactions of alkoxy radical/alcohol pairs.[27] Figure 6 shows two sets of VB-state curves, which are drawn differently, in unbroken black and dotted black lines. The regular VB states describe the normal HAT process, with promoted states that involve triplet decoupling of the O–H bond electrons and re-pairing the electron on H$^\bullet$ with the electron of the respective alkoxy radical. On the other hand, the dotted curves, which intersect along the same reaction coordinate, describe proton abstraction whereby the alkoxyl radical behaves as a base and abstracts the proton of the alcohol. These dotted VB curves correspond to the classical 4-electron/3-center reactions that have been amply described in

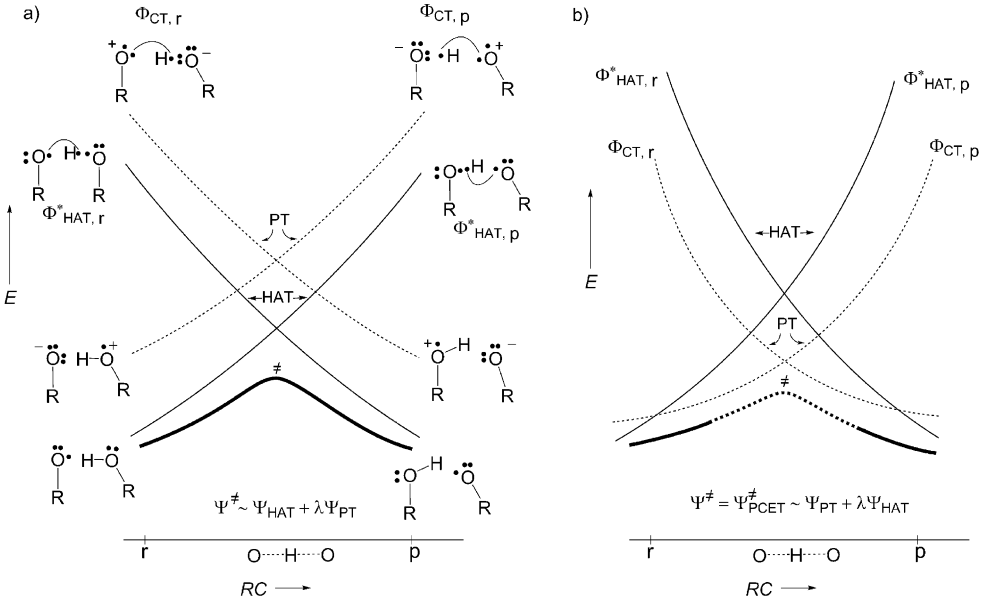

Figure 6. VBSCDs describing the hybrid HAT/PCET dichotomy to mixing of normal HAT VB states (black unbroken line), and proton transfer (PT) curves (dotted lines), along the reaction coordinate. For simplicity, only one oxygen lone pair that participates in the PCET is shown. The PCET curves are anchored in charge transfer (CT) promoted states of reactants and products, indicated as $\Phi_{CT,r}$ and $\Phi_{CT,p}$. a) A case where the CT states lie higher than the PT states. Assuming no symmetry restrictions, the wave function of the transition state ($\Psi^{\neq}$) has a dominant HAT character with a secondary PT character. b) A case where the CT curves are low-lying and descend below the crossing point of the HAT curves. The corresponding transition state is now a PCET-type with a predominant PT character and a secondary HAT character. The mixing of the two state-sets results in a smooth transformation from a PT to a HAT state, at the two diagram ends.

the past.[35c,48,71] Thus, the proton-transfer VB state curves are anchored in charge-transfer states of the reactants and products, $\Phi_{CT,r}$ and $\Phi_{CT,p}$, and correlate down to the corresponding proton-transferred reactants and products, which are higher than the corresponding HAT states of reactants and products. Another feature that should be noted is that as they are Lewis curves, the dotted curves contain implicitly the triple-ion VB structure ($O:^- H^+ {}^-:O$), and are hence more concave than the 3-electron/3-center curves.[35c,48,71]

Figure 6 describe two distinct cases. Figure 6a describes a case in which the Φ_{CT} states are higher in energy than the HAT states, and therefore the VB mixing generates a mixed-character transition state that has a dominant HAT character, and a secondary proton-transfer character, as shown by the expression of the wave function of the transition state, $\Psi^{\ddagger}$ (under Figure 6). In contrast, Figure 6b, shows the case where the charge-transfer states are lower than the HAT states, and especially so in the region of the avoided crossing, so that the VB mixing will establish a PCET transition state, $\Psi^{\ddagger}_{PCET}$. Thus, as a result of the VB mixing and avoided crossing, the corresponding transition state in Figure 6b will have a predominant proton-transfer character with a small HAT character. Furthermore, the VB mixing will cause a smooth transformation on the ground-state curve from proton-transfer to HAT characters, hence together a PCET process. Note that as the dotted-curves cross below the crossing point of the HAT curves, the corresponding transition state in Figure 6b will have a lower energy compared with the "normal" HAT case in Figure 6a.

The mechanistic choice will depend on the strength of the O–H bond, and the ionization energy (IE) of the lone pair in the RO$^{\bullet}$ radical. A strong O–H bond will be a poor electron acceptor,[33b,35c] and when the radical has a high $IE_{RO:}$, the two effects together generate high-lying charge-transfer states, and vice versa when the O–H bond is weak and the $IE_{RO:}$ is low. The O–H bonds of alkyl alcohols are approximately 20 kcal mol^{-1} stronger than O–H bonds of phenols, and the corresponding IE value for alkoxyl is higher than phenoxyl, and as such the PhO$^{\bullet}$/PhO-H pair proceeds by PCET (as in Figure 6b) whereas the $CH_3O^{\bullet}$/CH_3O-H pair undergoes simple HAT (as in Figure 6a). Clearly, unless there is a symmetry restriction of the VB mixing (which there should not be), a spectrum of cases can be expected that differ in the amounts of PCET and HAT character and depend on the chemical identity of the radical and the H-donor molecule. It is also clear from this analysis that a pair, such as $PhCH_2^{\bullet}$/$PhCH_3$ cannot participate in a PCET mechanism, firstly because the C–H bond is generally a very poor electron acceptor, and secondly since the radical does not have an electron pair with a sufficiently low IE to support low-enough charge-transfer states.

5.2. VB Models for HAT and PCET in Self H-Exchange by Closed-Shell Abstractors

Having discussed the HAT/PCET spectrum for an open-shell abstractor, we turn to the case of closed-shell abstractors, for example, MnO_4^- and CrO_2Cl_2. Figure 7 shows the VB diagram for the identity process of MnO_4^- with $MnO_3(OH)^{\bullet -}$, where the MnO_4^- abstractor is represented as a Mn=O: moiety, and the $MnO_3(OH)^{\bullet -}$ as $^{\bullet}$Mn-OH. As discussed for Figure 6, in this case as well, we have two sets of VB curves shown as an unbroken black line for the normal HAT process and a dotted line for the proton-transfer process. The charge-transfer promoted states for the dotted state curves are generated by one-electron transfer from MnO_4^- into the O–H bond of $MnO_3(OH)^{\bullet -}$. Since the ionization energy (IE) of MnO_4^- should not be too high (our calculated B3LYP/B1 $IE(MnO_4^-K^+)$ value is 70 kcal mol^{-1} lower than that of the lone pair of H_2O), while the electron affinity of $MnO_3(OH)^{\bullet -}$ may well be substantial,[74] the charge-transfer states should be below the HAT-promoted states. As a result, we would expect to find a PCET mechanism with a rather low barrier.

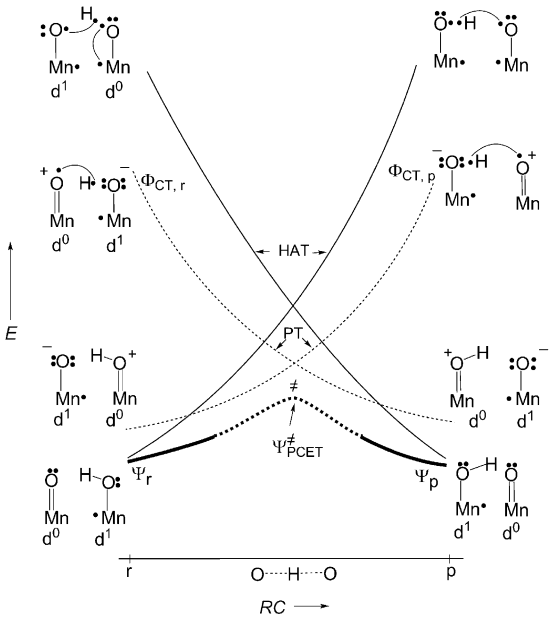

Figure 7. VBSCD describing the hybrid PCET mechanism of the self-H exchange reaction $MnO_4^- + MnO_3(OH)^{\bullet -} \rightarrow MnO_3(OH)^{\bullet -} + MnO_4^-$, based on the mixing and avoided crossing of normal HAT states (unbroken lines), and proton-transfer (PT) states (dotted lines). For simplicity only one lone pair is shown on oxygen.

A crude way of evaluating the barrier from the above VB diagram is to estimate the promotion gap as the energy difference between the ground state on the reactant side all the way to the excited charge-transfer state on the product side. Viewed in this manner, the process involves breaking the MnO–H bond of $MnO_3(OH)^{\bullet -}$, while at the same time creating a repulsive 3-electron interaction of the H$^{\bullet}$ species with the M–O: moiety of MnO_4^-. The repulsive 3-electron interaction has the same expression as the corresponding bond energy.[35c,e,53b,c] Therefore the approximate value of this promotion energy is given by Equation 15.

$$G_{PCET} \approx 2\,D_{OH} \tag{15}$$

And the VB barrier expression is thus given by Equation 16.

$$\Delta E^{\ddagger}{}_{VB,PCET} \approx f(2\,D_{OH}) - B;\ B = {}^1\!/_2\,BDE_{OH} \tag{16}$$

If we use the same f value as in HAT, that is, $f = 0.3$, we predict $\Delta E^{\neq}_{VB,PCET} = 17.0$ kcal mol^{-1}, while if we consider that the dotted curves are more concave as in 4-electron/3-center reactions,[35c] that is, $f \approx 0.25$, the predicted VB barrier is $\Delta E^{\neq}_{VB,PCET} = 7.4$ kcal mol^{-1}. The B3LYP/B1 value is 11.9 kcal mol^{-1} (see Figure 5a), while the estimated enthalpic barrier using Marcus analysis of the experimental data is, for example, 10.6 kcal mol^{-1}. A similar application to the identity reaction $CrO_2Cl_2/CrOCl_2(OH)^{\bullet}$ leads to $\Delta E^{\neq}_{VB,PCET}$ values which has lower and upper boundaries of 6.4 and 15.9 kcal mol^{-1}, while the experimentally estimated free energy barrier is 12.9 kcal mol^{-1}. Based on these two applications, a logical way of estimating these barriers is the use of an average f value, $f = 0.275$, as in Equation (17).

$$\Delta E^{\neq}_{VB,PCET} \approx 0.275\,(2\,D_{OH}) - B;\; B = {}^1\!/_2\,BDE_{OH} \qquad (17)$$

An average f is justifiable since because of VB mixing, the curves have hybrid PCET/HAT character corresponding to both 3-electron/3-center and 4-electron/3-center VB states (of course, this assumes that there is no symmetry restriction on the PCET/HAT mixing). Employing the average f values leads to the VB-predicted barriers, summarized in Scheme 5 along with the barriers extracted from the Marcus equation from experimental data [Eq. (3a)], and the B3YLP/B1 values. The agreement is satisfactory.

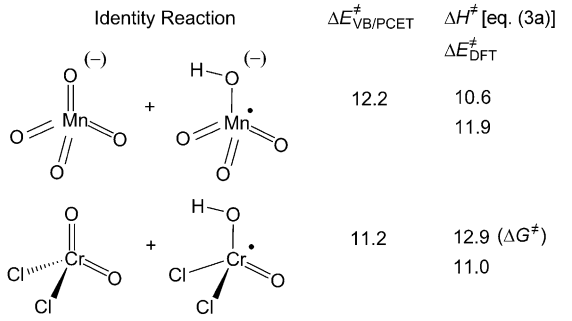

Scheme 5. VB barriers (kcal mol^{-1}) predicted using Equation (17) along with those derived from the Marcus equation and B3LYP/B1 computed values for the PCET self H-exchange reactions of MnO_4^- and CrO_2Cl_2.

5.3. VB Models for Hybrid HAT/PCET Mechanisms in Non-Identity H-Abstraction by Closed-Shell Abstractors

We are now ready to consider the hybrid HAT/PCET mechanism in non-identity H-abstractions where both the abstractor and the substrate are closed-shell molecules, such as MnO_4^-, CrO_2Cl_2, or α-methylstyrene reacting with a generically labeled H–Y molecule. In these cases, the charge-transfer (CT) states of reactants and products depend on whether the abstractor and the H-donor molecules carry electron pairs that can sustain low-lying charge-transfer states that may compete with the HAT states. In Figure 8 we consider two such cases.

Figure 8a depicts the HAT (black unbroken line) and charge-transfer (dotted lines) states for generic closed-shell metal oxo abstractor and H–Y. We consider two charge-transfer states that mediate proton abstraction from H–Y. The $\Phi_{CT,r}$ state on the reactant side involves an electron transfer from the oxygen lone pair to the H–Y bond, and correlates down to the proton-transferred product state, $\Phi_{PT,p}$. The $\Phi_{CT,p}$ state on the product side involves an electron transfer from the Y$^{\bullet}$ radical (assuming we have an alkyl radical, such as C_6H_{11} in which there are no low-lying electron pairs) into the O–H bond of the MO–H moiety, and correlate down to the proton-transferred reactant state, $\Phi_{PT,r}$. These two charge-transfer state curves are generally quite high in energy, and will remain above the crossing point of the normal HAT curves, but by mixing into the HAT curves they will generate a transition state with a hybrid HAT/proton-transfer character (hence having some PCET character).[75]

Figure 8b depicts the HAT (black unbroken line) and charge-transfer (dotted line) states for a generic closed-shell olefin abstracting an H-atom from H–Y. The charge-transfer states are analogous to the ones in Figure 8a, with one difference that now the same electron pair, the π-bond, is responsible for both the HAT and the charge-transfer state, $\Phi_{CT,r}$; in the HAT state the π-bond is decoupled into a triplet

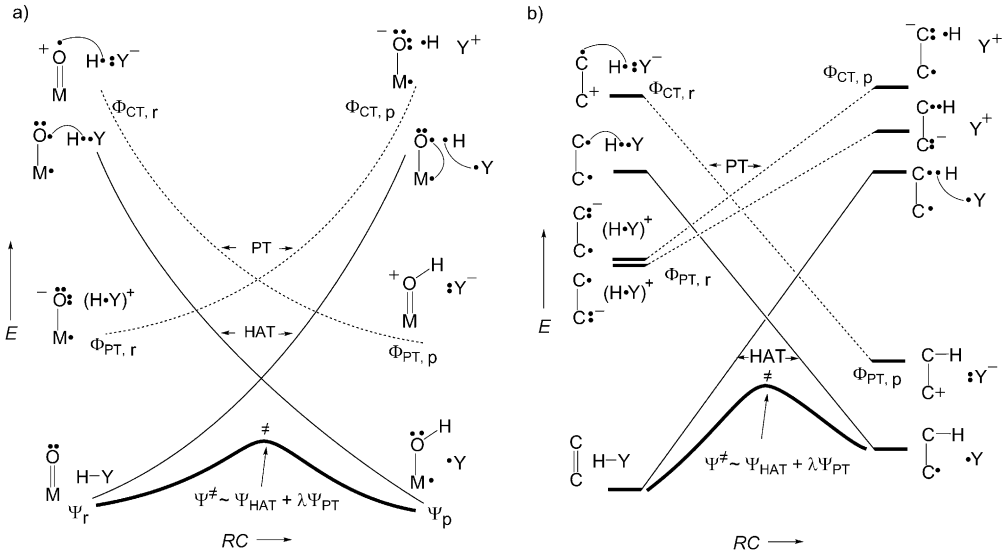

Figure 8. VBSCDs describing the HAT/PCET hybrid character for reactions of closed-shell abstractors and a molecule H–Y: a) The abstractor molecule is a closed-shell metal oxo reagent. For simplicity only one lone-pair is drawn on oxygen . b) The abstractor is an olefin. In both cases, the transition states have hybrid characters resulting from the mixing of the PT curves (dotted lines) into the HAT curves (black unbroken lines).

while in the charge-transfer state the π-bond transfers an electron to the H–Y bond. On the product side, the $\Phi_{PT,p}$ state is generated by an electron transfer from the radical Y• into the C–H bond, and by transferring the electron into the adjacent carbon with triplet decoupling of the C–H bond. As in Figure 8a, in this case as well the two charge-transfer state curves are higher than the crossing point of the HAT curves, and by mixing will introduce some PCET character into the corresponding transition state.

All in all, Figure 8 shows that for a given abstractor the PCET character depends on the H–Y molecule. Thus, for a molecule with a strong Y–H bond, such as C_6H_{12}, the $\Phi_{CT,r}$ state will be high in energy, and the ionization energy of Y• will be quite large, making $\Phi_{CT,p}$ high as well. As such, the amount of PCET character in the transition state is expected to be small, and the reaction may be treated like a normal HAT (see Figure 4a) in which the closed-shell abstractor pays the penalty of preparing the abstractor site with a radical (through the HAT states). On the other hand, when the H–Y bond is weak, such as in DHA, and the corresponding radical has a low ionization energy, the charge-transfer states will be lower in energy, and the resulting PCET character in the transition state may well be significant. Thus, while the identity reaction of the abstractor, for example, MnO_4^-/$MnO_3(OH)^{\bullet-}$ is by itself a PCET process (Figure 7), the corresponding non-identity reactions will have a HAT character with a variable but secondary PCET character (assuming no symmetry restrictions on the VB mixing). This is the reason why application of the Marcus equation (see above) to different reactions, such as MnO_4^-/$PhCH_3$ versus MnO_4^-/DHA or of CrO_2Cl_2/C_6H_{12} versus $CrO_2Cl_2/PhCH_3$ and CrO_2Cl_2/DHA will yield different identity barriers, as we showed above in Table 2 and the associated discussion. This situation is what we referred to above as the dichotomy of closed-shell abstractors, and now we outlined this dichotomy based on clear electronic structure principles. Thus, the identity barriers of closed-shell abstractors, such as MnO_4^- and CrO_2Cl_2, do not always carry over uniquely to the non-identity reactions and depend strongly on the reaction partner. Consequently, different non-identity reactions of the same abstractor with a series of H-donor molecules will reveal a variable identity barrier, for the abstractor, differing from one reaction to the other, and depending on the H-donor molecule.

Strictly speaking, according to Figure 8, the more significant PCET character means that the transition state has larger resonance energy, *B*. Including this feature in the VB model is possible, as shown recently for aromatic activation by P450,[39c] but this requires a more complex treatment which we avoid herein. Instead, we can highlight this dichotomy, using the limiting cases of HAT versus PCET as shown in Scheme 6 for two reactions CrO_2Cl_2/C_6H_{12} versus CrO_2Cl_2/$PhCH_3$. Thus, for each case we present the predicted VB barriers using the pure HAT limit in Figure 4a, where the closed-shell abstractor must pay the additional promotion energy, $3/8\,f\Delta E_{ST}$ [Eq. (12)], during C–H activation, and the pure PCET limit where the additional promotion energy can be excluded.

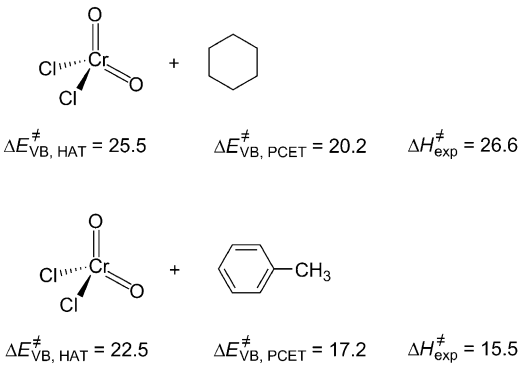

Scheme 6. Predicted VB barriers (kcal mol^{-1}) at the pure HAT ($\Delta E^{\neq}_{VB,HAT}$) and PCET ($\Delta E^{\neq}_{VB,PCET}$) limits, and the experimental enthalpies of activation ($\Delta H^{\neq}_{exp}$) for CrO_2Cl_2/C_6H_{12} and $CrO_2Cl_2/PhCH_3$.

For cyclohexane, the C–H bonds are strong and the ionization energy of the radical C_6H_{11} is correspondingly high, the VB predicted barrier for the HAT limit, $\Delta E^{\neq}_{VB,HAT}$, is closer to the experimental enthalpy of activation, $\Delta H^{\neq}_{exp}$, than the VB-predicted barrier for the pure PCET limit, $\Delta E^{\neq}_{VB,PCET}$ (see Scheme 6). In contrast, for toluene,[76,77] with the weaker C–H bond and lower ionization energy for the corresponding radical, the barrier for the pure PCET limit is closer to the experimental $\Delta H^{\neq}_{exp}$ value. Using experimentally based BDE (*D*) and ΔE_{ST} parameters leads to higher VB barriers, but with a similar trend. Clearly, in this form, the VB model cannot predict "how much" HAT or PCET character a given reaction will have, however the model can still predict trends. Thus, the model shows that the PCET character in a HAT process will vary as a function of the strength of the C–H bond (Y–H in general) and the ionization energy of the radical (of Y• in general), which will determine the energies of the charge-transfer states that mix into the HAT states. Whenever the H–Y bond is weak and the corresponding radical of the substrate has a low ionization potential, the charge-transfer states will be lower in energy and will endow the transition state with a higher PCET character (assuming no symmetry restriction for VB mixing). Such a series, with a variable PCET character, is predicted to give rise to different identity barriers for the same identity process using the Marcus equation.

Once we comprehend that the PCET character is due to charge-transfer (CT) states which mix into the HAT states, we may envision other such states. For example, molecules such as xanthene and nicotinamide adenine nucleotide hydride (NADH), have weak C–H bonds, which are good electron donors (low ionization energy),[78] and radicals that are good electron acceptors. As such, charge-transfer states that are generated by electron transfer from the C–H bond into a vacant orbital of the abstractor and correlate to the hydride-transfer state may also contribute to reactivity.

6. Limitations and Prospects of the VB model

At this stage the VB model is simple to apply. For normal HAT reactions of open-shell abstractors, all that is needed is

a set of BDE and D values [Eqs. (10), (11)]. Using Equation (10a) for the VB barrier $\Delta E^{\neq}_{VB}(1)$ without the quadratic term, and the expressions of D [Eq. (6)], we can write the barrier as Equation (18).

$$\Delta E^{\neq}_{VB}(1) \approx 0.3\,(|RE_{X\cdot}| + |RE_{Y\cdot}|) + 0.55\,BDE_{H\text{-}X} - 0.45\,BDE_{H\text{-}Y} + [0.1125\,\Delta E_{ST}] \quad (18)$$

$|RE_{Y\cdot}|$ and $|RE_{X\cdot}|$ are the radical reorganization energy terms, which gauge the extent of radical declocalization, and contribute to barriers arising from the need to "prepare" the radicals (X$^{\cdot}$ and Y$^{\cdot}$) for bonding. The subsequent two terms provide the contribution of bond cleavage versus bond formation. When the abstractor is a closed-shell molecule, the normal HAT will also be required to pay the $0.1125\,\Delta E_{ST}$ cost of the additional promotion energy, which accounts for the "preparation" of the closed-shell molecule for H-abstraction [Figure 4a, Eq. (12)]; this term is given in square brackets. The PCET limit can be tested using Equation (17), which requires only BDE and D values.

Of course, with such simplicity we cannot expect the model to be infallible. Our experience shows that the VB model overestimates barriers for reactions which have very small barriers, as for example, in highly exothermic reactions, and in the higher homologue identity reactions, X/HX′ (X = Br, I, SH). In such cases, it is better to use BDE and D values which do not include ZPE corrections, and then subtract the ZPE difference from the classical barrier (for reactants and transition state). When radicals are extremely delocalized, such as, the 1,4-cyclohexadienyl radical, the radical reorganization energy term as defined by Equation (6), will be underestimated, and will cause some underestimation of the corresponding HAT barrier. The model also overestimates the barriers for H-abstractions from O–H and N–H bonds, which tend towards PCET. Another limitation is that our formula for the resonance energy of the transition state, B [Eq. (10a)] does not include the effects of mixing of secondary states as, for example, in the cases with variable PCET character. And lastly, let us mention the lack of tunneling, which is not part of the model. Despite these limitations, the model is attractive and allows the user to collect BDE/D and ΔE_{ST} data and estimate reasonable barriers with extreme ease, either from experimentally based BDE/D data or from calculated ones.

The lack of tunneling is a limitation, which is difficult to rectify, but the other limitations can be addressed in future developments of the model. For example, realistic reorganization energies for highly delocalized radicals can be obtained by using the proper promotion terms that localizes the radicals. The ability to use variable transition-state resonance energy requires a derivation of the second-order effect of mixing of charge-transfer states into the HAT transition state, as done for arene activation by Cpd I in which the charge-transfer states may mix prominently into the normal radical-activation transition state.[39c] Such a formulation for the HAT reaction may allow us to bridge effectively the HAT/PCET limits and present a unified theory for the entire reaction spectrum.

Another future prospect is the unification of the VB model to treat the chemoselectivity that closed-shell reagents, such as CrO_2Cl_2, MnO_4^-, and other metal oxides exhibit with an alkene. These pathways are depicted in Scheme 7 for CrO_2Cl_2, but are general for all closed-shell reagents.

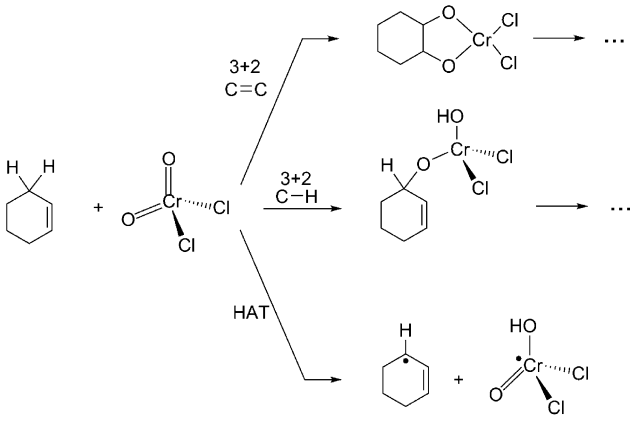

Scheme 7. Regiochemical pathways for the reaction of a closed-shell reagent, such as CrO_2Cl_2, with cyclohexene.

These are 3+2 cycloaddition to the C=C bond, abstraction of the allylic H, and concerted addition of the allylic C–H bond across the Cr=O bond.[63] A simple application of the VB model shows that the oxidative 3+2 cycloaddition will have a promotion gap, $G_r \approx 150$ kcal mol^{-1}, and hence a barrier of approximately 10 kcal mol^{-1} which is much lower than for H-abstraction (for which G_r is typically 250 kcal mol^{-1}). Why then should CrO_2Cl_2 not react in a concerted manner with a C–H bond, without leading to radicals? Refinement of the VB model to enable it to treat this array of problems is a future challenge.

7. Summary and Outlook

The Review utilizes the valence bond (VB) model developed by one of the authors in 1981[35a] and reviewed in for organic reactions in 1999,[35c] and recently, for key reactions of cytochrome P450.[39b] This growing repertoire has enabled us to present herein a unified treatment of H-abstraction. As such, the Review shows the generality and unifying power of the VB model for understanding H-abstraction reactivity starting from the simplest $H + H_2$ process, through organic and main-group element reactions, and all the way to P450 hydroxylations and H-transfers among closed-shell molecules; altogether well over 50 reactions are treated and their barriers are estimated from raw data. Furthermore, an attractive feature of the model is the creation of a natural bridge to the Marcus equation. Thereby the model enables intrinsic barriers and identity barriers to be calculated from raw data, and answers key questions about the origins of these barriers and their heights.

A key goal of the Review is to address the surging interest in H-abstraction by closed-shell abstractors, and answer the

question, "*is there a need to have a radical center at the abstractor in order to abstract a hydrogen atom*"? The answer to this question is, "*of course not*", but if the abstractor is a closed-shell molecule then in the normal HAT event, this will require a high barrier[79] owing to the additional promotion energy that is required to create a radical and prepare the abstractor for H-abstraction [Figure 4 a,b, Eqs. (12), (18)]. It is important to realize that this question has been posed in the literature,[26b,c,28] because H-abstraction rate constants of closed-shell abstractors were found to fall on the same BEP plot as the reactions of radical abstractors, such as OH$^{\bullet}$, *t*BuOO$^{\bullet}$, using the BDE_{OH} of the O–H bond in the products, as the organizing quantity. The linear correlation with the bond dissociation energy of the O–H bond has been taken as proof that the radical character is unimportant for HAT. But it is of course not a proof,[80] since the BDE_{OH} quantity for the closed-shell abstractors already incorporates the cost of decoupling the bonds of the closed-shell abstractors and preparing them for abstracting an H atom. In fact, the open-shell and closed-shell abstractors lie on the same line because the closed-shell abstractors pay the penalty of preparing a radical at the abstractor center along the reaction path.

Our attempts to answer this leading question (is a radical needed…?) has revealed to us that small barriers for closed-shell abstractors are encountered whenever the abstractor has a way to avoid this excess promotion energy while at the same time abstracting a hydrogen atom. This is done through the alternative path of concerted proton-coupled electron transfer (PCET). The VB modeling of the PCET and HAT has revealed the importance of the mixed HAT/PCET reaction, and equations were derived to estimate barriers for the two limiting cases, using raw data. The VB modeling shows that the HAT/PCET dichotomy will cause the Marcus analysis to produce different identity barriers for the same identity reaction (X + H–X$^{\bullet}$) in different nonidentity processes (X + H–Y). Comparison of the reactions of CrO_2Cl_2 with cyclohexane and toluene is a case in point. Generally speaking, prominent PCET character in non-identity reactions will be limited to substrates with very weak H–Y bonds and low ionization energy of the Y$^{\bullet}$ radical. It will not be observed for strong Y–H bonds with Y groups that have moderate to high ionization energy for the corresponding radical.

Still, despite the above unity, the limitations and prospects described shows that the story is not yet complete, and as the title suggests there are still parts missing from the great jigsaw puzzle of a most widespread reaction in nature.

Sason Shaik acknowledges support by the Israel Science Foundation (ISF Grant 53/09) and a special grant from Minerva. We gratefully thank Prof. Dr. Helmut Schwarz for enlightening comments during the preparation of the manuscript. Dr. Maria Schlangen is warmly thanked for the translation into German.

Received: November 29, 2011
Published online: May 4, 2012

[1] a) *Biomimetic Oxidations Catalyzed by Transition Metal Complexes* (Ed.: B. Meunier), Imperial College Press, London, **2000**; b) "Metal-Oxo and Metal-Peroxo Species in Catalytic Oxidations": *Structure & Bonding*, *Vol. 97* (Ed.: B. Meunier), Springer, Berlin, **2000**, pp. 1–323.

[2] a) P. R. Ortiz de Montellano, *Chem. Rev.* **2010**, *110*, 932–948; b) J. T. Groves in *Cytochrome P450*: *Structure*, *Mechanism*, *and Biochemistry*, *3rd ed.* (Ed.: P. R. Ortiz de Montellano), Kluwer Academic/Plenum Publishers, New York, **2005**, chap. 1, pp. 1–43; c) J. T. Groves, *J. Chem. Educ.* **1985**, *62*, 928–931; d) W.-D. Woggon, *Top. Curr. Chem.* **1996**, *184*, 39–96; e) P. R. Ortiz de Montellano, J. J. de Voss, *Nat. Prod. Rep.* **2002**, *19*, 477–493; f) J. H. Dawson, M. Sono, *Chem. Rev.* **1987**, *87*, 1255–1276.

[3] For recent theoretical treatments, see: a) K. Yoshizawa, *Coord. Chem. Rev.* **2002**, *226*, 251–259; b) S. Shaik, S. Cohen, Y. Wang, H. Chen, D. Kumar, W. Thiel, *Chem. Rev.* **2010**, *110*, 949–1017; c) B. Meunier, S. P. de Visser, S. Shaik, *Chem. Rev.* **2004**, *104*, 3947–3980; d) S. Shaik, D. Kumar, S. P. de Visser, A. Altun, W. Thiel, *Chem. Rev.* **2005**, *105*, 2279–2328; e) S. Shaik, F. Ogliaro, S. P. de Visser, D. Schröder, H. Schwarz, *Curr. Opin. Chem. Biol.* **2002**, *6*, 556–567; f) H. M. Senn, W. Thiel, *Angew. Chem.* **2009**, *121*, 1220–1254; *Angew. Chem. Int. Ed.* **2009**, *48*, 1198–1229.

[4] See, for example, F. P. Guengerich in *Cytochrome P450*: *Structure*, *Mechanisms*, *and Biochemistry*, *2nd ed.*, (Ed.: P. R. Ortiz de Montellano), Plenum, New York, **1995**.

[5] a) C. Colas, P. R. Ortiz de Montellano, *Chem. Rev.* **2003**, *103*, 2305–2332; b) H. B. Dunford, *Heme Peroxidases*, Wiley-VCH, New York, **1999**; c) H. U. Markwalder, H. Neukom, *Phytochemistry* **1976**, *15*, 836–837.

[6] a) E. T. Denisov, T. G. Denisova, *Handbook of Antioxidants*, CRC, New York, **2000**; b) *Reactive Oxygen Species* (Ed.: C. C. Chiueh), The New York Academy of Sciences, New York, **2000**; c) J. Stubbe, W. A. van der Donk, *Chem. Rev.* **1998**, *98*, 705–762; d) Radicals in Enzymatic Catalysis—a Thermodynamic perspective, in: J. Hioe, H. Zipse, *Faraday Discuss.* **2010**, *145*, 301–310.

[7] See, for example, a) W. Nam, *Acc. Chem. Res.* **2007**, *40*, 465; b) C. Krebs, D. G. Fujimori, C. T. Walsh, J. M. Bollinger, Jr., *Acc. Chem. Res.* **2007**, *40*, 484–492; c) W. Nam, *Acc. Chem. Res.* **2007**, *40*, 522–531; d) C. Kim, Y. Dong, L. Que, Jr., *J. Am. Chem. Soc.* **1997**, *119*, 3635–3636; e) G. Xue, R. de Hont, E. Münck, L. Que, Jr., *Nat. Chem.* **2010**, *2*, 400–405; f) B. G. Fox, K. S. Lyle, C. E. Rogge, *Acc. Chem. Res.* **2004**, *37*, 421–429; g) P. H. Buist, *Nat. Prod. Rep.* **2004**, *21*, 249–262; h) B. Behrouzian, P. H. Buist, *Curr. Opin. Chem. Biol.* **2002**, *6*, 577–582; i) M.-H. Baik, M. Newcomb, R. A. Friesner, S. J. Lippard, *Chem. Rev.* **2003**, *103*, 2385–2419.

[8] For non-heme complexes and their reactions see, a) J.-U. Rohde, J.-H. In, M. H. Lim, W. W. Brennessel, M. R. Bukowski, A. Stubna, E. Münck, W. Nam, L. Que, Jr., *Science* **2003**, *299*, 1037–1039; b) J. Kaizer, E. J. Klinker, N. Y. Oh, J.-U. Rohde, W. J. Song, A. Stubna, J. Kim, E. Münck, W. Nam, L. Que, Jr., *J. Am. Chem. Soc.* **2004**, *126*, 472–473.

[9] See, for example, a) D. Schröder, H. Schwarz, *Angew. Chem.* **1995**, *107*, 2126–2150; *Angew. Chem. Int. Ed. Engl.* **1995**, *34*, 1973–1995; b) H. Schwarz, *Int. J. Mass Spectrom.* **2004**, *237*, 75–105; c) N. Dietl, C. van der Linde, M. Schlangen, M. K. Beyer, H. Schwarz, *Angew. Chem.* **2011**, *123*, 5068–5072; *Angew. Chem. Int. Ed.* **2011**, *50*, 4966–4969; d) H. Schwarz, *Angew. Chem.* **2011**, *123*, 10276–10297; *Angew. Chem. Int. Ed.* **2011**, *50*, 10096–10115; e) E. Rezabal, J. Gauss, J. M. Matxain, R. Berger, M. Diefenbach, M. C. Holthausen, *J. Chem. Phys.* **2011**, *134*, 064304; f) H. Shiota, K. Yoshizawa, *J. Am. Chem. Soc.* **2000**, *122*, 12317–12326.

[10] For some recent Reviews, see: a) D. Balcells, E. Clot, O. Eisenstein, *Chem. Rev.* **2010**, *110*, 749–823; b) J. Roithová, D. Schröder, *Chem. Rev.* **2010**, *110*, 1170–1211; c) C. Coperet,

Chem. Rev. **2010**, *110*, 656 – 680; d) T. Newhouse, P. S. Baran, *Angew. Chem.* **2011**, *123*, 3422 – 3435; *Angew. Chem. Int. Ed.* **2011**, *50*, 3362 – 3374; e) A. Gunay, K. H. Theopold, *Chem. Rev.* **2010**, *110*, 1060 – 1081.

[11] G. A. Olah, A. Molnar, *Hydrocarbon Chemistry*, Wiley, New York, **1995**.

[12] J. S. Francisco, M. M. Maricq, *Acc. Chem. Res.* **1996**, *29*, 391 – 397, and references therein.

[13] A. A. Fokin, P. R. Schreiner, *Chem. Rev.* **2002**, *102*, 1551 – 1593.

[14] See, for example, metalo oxyl species with radical character, a) D. Balcells, C. Raynaud, R. H. Crabtree, O. Eisenstein, *Inorg. Chem.* **2008**, *47*, 10090 – 10099; b) D. Balcells, C. Raynaud, R. H. Crabtree, O. Eisenstein, *Chem. Commun.* **2009**, 1772 – 1774; c) D. Balcells, C. Raynaud, R. H. Crabtree, O. Eisenstein, *Chem. Commun.* **2008**, 774 – 746; d) S. Ye, F. Neese, *Proc. Natl. Acad. Sci. USA* **2011**, *108*, 1228 – 1233; e) E. I. Solomon, S. D. Wong, L. V. Liu, A. Becker, M. S. Chow, *Curr. Opin. Chem. Biol.* **2009**, *13*, 99 – 113; f) X.-L. Ding, X.-N. Wu, Y.-X. Zhao, S.-G. He, *Acc. Chem. Res.* **2012**, *45*, 382 – 390.

[15] a) K. Chen, Z.-C. Wang, M. Schlangen, Y.-D. Wu, X. H. Zhang, H. Schwarz, *Chem. Eur. J.* **2011**, *17*, 9619 – 9625; b) N. Dietl, R. F. Höckendorf, M. Schlangen, M. Lerch, M. K. Beyer, H. Schwarz, *Angew. Chem.* **2011**, *123*, 1466 – 1470; *Angew. Chem. Int. Ed.* **2011**, *50*, 1430 – 1434; c) N. Dietl, M. Engeser, H. Schwarz, *Angew. Chem.* **2009**, *121*, 4955 – 4957; *Angew. Chem. Int. Ed.* **2009**, *48*, 4861 – 4863; d) D. Schröder, J. Roithová, *Angew. Chem.* **2006**, *118*, 5835 – 5838; *Angew. Chem. Int. Ed.* **2006**, *45*, 5705 – 5708; e) A. Božović, D. K. Bohme, *Phys. Chem. Chem. Phys.* **2009**, *11*, 5940 – 5951; f) Z.-C. Wang, T. Weiske, R. Kretschmer, M. Schlangen, M. Kaupp, H. Schwarz, *J. Am. Chem. Soc.* **2011**, *133*, 16930 – 16937.

[16] a) K. B. Wiberg, G. Foster, *J. Am. Chem. Soc.* **1961**, *83*, 423 – 429; b) K. B. Wiberg, R. Eisenthal, *Tetrahedron* **1964**, *20*, 1151 – 1161.

[17] a) G. K. Cook, J. M. Mayer, *J. Am. Chem. Soc.* **1994**, *116*, 1855 – 1868; b) G. K. Cook, J. M. Mayer, *J. Am. Chem. Soc.* **1995**, *117*, 7139 – 7156; c) K. A. Gardner, J. M. Mayer, *Science* **1995**, *269*, 1849 – 1851; d) J. M. Mayer, *Acc. Chem. Res.* **1998**, *31*, 441 – 450; e) For reactions of MnO_4^-, see: K. A. Gardner, L. L. Kuehert, J. M. Mayer, *Inorg. Chem.* **1997**, *36*, 2069 – 2078. The activation free energies are taken from Table 1 (the columns "values for the H· transfer step"). The activation enthalpies were derived from the corresponding free energies.

[18] C. Rüchardt, M. Gerst, M. Nöltke, *Angew. Chem.* **1992**, *104*, 1516 – 1518; *Angew. Chem. Int. Ed. Engl.* **1992**, *31*, 1523 – 1525.

[19] a) C. Limberg, *Chem. Eur. J.* **2000**, *6*, 2083 – 2089; b) T. Wistuba, C. Limberg, P. Kirchner, *Angew. Chem.* **1999**, *111*, 3222 – 3224; *Angew. Chem. Int. Ed.* **1999**, *38*, 3037 – 3039.

[20] P. J. Wagner, Y. Zhang, A. E. Puchalski, *J. Phys. Chem.* **1993**, *97*, 13368 – 13374.

[21] a) K. A. Prokop, S. P. de Visser, D. P. Goldberg, *Angew. Chem.* **2010**, *122*, 5217 – 5221; *Angew. Chem. Int. Ed.* **2010**, *49*, 5091 – 5095; b) T. Kojima, Y. Hirai, T. Ishizuka, Y. Shiota, K. Yoshizawa, K. Ikemura, T. Ogura, S. Fukuzumi, *Angew. Chem.* **2010**, *122*, 8627 – 8631; *Angew. Chem. Int. Ed.* **2010**, *49*, 8449 – 8453.

[22] a) D. Schröder, S. Shaik, *Angew. Chem.* **2011**, *123*, 3934 – 3935; *Angew. Chem. Int. Ed.* **2011**, *50*, 3850 – 3851; b) T. Kojima, S. Fukuzumi, *Angew. Chem.* **2011**, *123*, 3936 – 3937; *Angew. Chem. Int. Ed.* **2011**, *50*, 3852 – 3853.

[23] a) N. Jin, J. T. Groves, *J. Am. Chem. Soc.* **1999**, *121*, 2923 – 2924; b) N. Jin, J. L. Bourassa, J. L. Tizio, J. T. Groves, *Angew. Chem.* **2000**, *112*, 4007 – 4009; *Angew. Chem. Int. Ed.* **2000**, *39*, 3849 – 3851; c) F. De Angelis, N. Jin, R. Car, J. T. Groves, *Inorg. Chem.* **2006**, *45*, 4268 – 4276.

[24] A. M. Khenkin, D. Kumar, S. Shaik, R. Neumann, *J. Am. Chem. Soc.* **2006**, *128*, 15451 – 15460.

[25] C. R. Waidmann, X. Zhou, E. A. Tsai, W. Kaminsky, D. A. Horvat, W. T. Bordern, J. M. Mayer, *J. Am. Chem. Soc.* **2009**, *131*, 4729 – 4743.

[26] For some general references on PCET mechanisms. See: a) R. I. Cukier, D. G. Nocera, *Annu. Rev. Phys. Chem.* **1998**, *49*, 337 – 339; b) J. Stubbe, D. G. Nocera, C. S. Yee, M. C. Y. Chang, *Chem. Rev.* **2003**, *103*, 2167 – 2201; c) J. M. Mayer, *Annu. Rev. Phys. Chem.* **2004**, *55*, 363 – 390; d) M. Sjödin, S. Styring, B. Åkermark, L. Sun, L. Hammarström, *J. Am. Chem. Soc.* **2000**, *122*, 3932 – 3936; e) J. Stubbe, W. A. van der Donk, *Chem. Rev.* **1998**, *98*, 705 – 762; f) S. Hammes-Schiffer, *Acc. Chem. Res.* **2001**, *34*, 273 – 281; g) For PCET/HAT relationships see: O. Tishchenko, D. G. Truhlar, A. Ceulemans, M. T. Nguyen, *J. Am. Chem. Soc.* **2008**, *130*, 7000 – 7101.

[27] a) J. M. Mayer, D. A. Horvat, J. L. Thomas, W. T. Borden, *J. Am. Chem. Soc.* **2002**, *124*, 11142 – 11147; b) M. Lingwood, J. R. Hammond, D. A. Horvat, J. M. Mayer, W. T. Borden, *J. Chem. Theory Comput.* **2006**, *2*, 740 – 745.

[28] a) J. S. Roth, J. C. Yoder, T.-J. Won, J. M. Mayer, *Science* **2001**, *294*, 2524 – 2526; b) J. M. Mayer, *Acc. Chem. Res.* **2011**, *44*, 36 – 46; c) J. M. Mayer, *J. Phys. Chem. Lett.* **2011**, *2*, 1481 – 1489; d) J. J. Warren, J. M. Mayer, *Proc. Natl. Acad. Sci. USA* **2010**, *107*, 5282 – 5287; e) see also the Supporting Information for Ref. [28d]; f) V. W. Manner, A. D. Lindsay, E. A. Mader, J. N. Harvey, J. M. Mayer, *Chem. Sci.* **2012**, *3*, 230 – 243.

[29] a) R. A. Marcus, *J. Am. Chem. Soc.* **1969**, *91*, 7224 – 7225; b) R. A. Marcus, *J. Phys. Chem.* **1968**, *72*, 891 – 899.

[30] a) R. P. Bell, *Proc. R. Soc. London Ser. A* **1936**, *154*, 414 – 429; b) M. G. Evans, M. Polanyi, *Trans. Faraday Soc.* **1938**, *34*, 11 – 24.

[31] For a derivation of the family of related equations see, J. R. Murdoch, *J. Am. Chem. Soc.* **1983**, *105*, 2159 – 2164.

[32] a) For a derivation using the properties of kinetic energy and the virial theorem, see, J. R. Murdoch, *J. Am. Chem. Soc.* **1982**, *104*, 588 – 600; b) for a derivation using a thermodynamic balancing condition and resulting energy additivity, see J. R. Murdoch, D. E. Magnoli, *J. Am. Chem. Soc.* **1982**, *104*, 3792 – 3800; c) for a related thermodynamic derivation, see, M. A. Ratner, R. D. Levine, *J. Am. Chem. Soc.* **1980**, *102*, 4898 – 4900.

[33] a) D. E. Magnoli, J. R. Murdoch, *J. Am. Chem. Soc.* **1981**, *103*, 7465 – 7469; b) S. Shaik, H. B. Schlegel, S. Wolfe, *Theoretical Aspects of Physical Organic Chemistry: The S_N2 Mechanism*, Wiley, New York, **1992**, pp. 33 – 41 and pp. 225 – 228; c) H. Mayr, M. Breugst, A. R. Ofial, *Angew. Chem.* **2011**, *123*, 6598 – 6634; *Angew. Chem. Int. Ed.* **2011**, *50*, 6470 – 6505; d) S. Hoz, H. Basch, J. L. Wolk, T. Hoz, E. Rozental, *J. Am. Chem. Soc.* **1999**, *121*, 7724 – 7725; e) M. Gonzales, W. D. Allen, H. F. Schaefer III, *J. Phys. Chem. A* **2005**, *109*, 10613 – 10628; f) E. Uggerud, *J. Phys. Org. Chem.* **2006**, *19*, 461 – 466; g) S. Wolfe, D. J. Mitchell, H. B. Schlegel, *J. Am. Chem. Soc.* **1981**, *103*, 7694 – 7696; h) For an extended Marcus analysis and LEPS modeling (with affinity to the VB approach) of hydride transfer of ca. 50 reactions, see: Y. Kim, D. G. Truhlar, M. M. Kreevoy, *J. Am. Chem. Soc.* **1991**, *113*, 7837 – 7847.

[34] a) S. S. Shaik, P. C. Hiberty, G. Ohanessian, J. M. Lefour, *J. Phys. Chem.* **1988**, *92*, 5086 – 5094; b) P. Maitre, P. C. Hiberty, G. Ohanessian, S. S. Shaik, *J. Phys. Chem.* **1990**, *94*, 4089 – 4093; c) S. Shaik, W. Wu, K. Dong, L. Song, P. C. Hiberty, *J. Phys. Chem. A* **2001**, *105*, 8226 – 8235; d) L. Song, W. Wu, K. Dong, P. C. Hiberty, S. Shaik, *J. Phys. Chem. A* **2002**, *106*, 11361 – 11370; e) L. Song, W. Wu, P. C. Hiberty, D. Danovich, S. Shaik, *Chem. Eur. J.* **2003**, *9*, 4540 – 4547; f) P. Su, L. Song, W. Wu, P. C. Hiberty, S. Shaik, *J. Am. Chem. Soc.* **2004**, *126*, 13539 – 13549.

[35] a) S. S. Shaik, *J. Am. Chem. Soc.* **1981**, *103*, 3692 – 3701; b) S. S. Shaik, *Prog. Phys. Org. Chem.* **1985**, *15*, 197 – 337; c) S. Shaik, A. Shurki, *Angew. Chem.* **1999**, *111*, 616 – 657; *Angew. Chem. Int. Ed.* **1999**, *38*, 586 – 625; d) S. Shaik, *Phys. Chem. Chem. Phys.*

2010, *12*, 8706 – 8720; e) S. Shaik, P. C. Hiberty, *A Chemist's Guide to Valence Bond Theory*, Wiley, New York, **2008**.

[36] A. Pross, *Theoretical and Physical Principles of Organic Reactivity*, Wiley, New York, **1995**.

[37] a) M.-D. Su, S.-Y. Chu, *Inorg. Chem.* **1998**, *37*, 3400 – 3406; b) M.-D. Su, S.-Y. Chu, *J. Am. Chem. Soc.* **1997**, *119*, 10178 – 10185; c) M.-D. Su, *Inorg. Chem.* **1995**, *34*, 3829 – 3832.

[38] a) Y. Wang, O. Haze, J. P. Dinnocenzo, S. Farid, R. S. Farid, I. R. Gould, *J. Phys. Chem. A* **2008**, *112*, 13088 – 13094; b) Y. Wang, O. Haze, J. P. Dinnocenzo, S. Farid, R. S. Farid, I. R. Gould, *J. Org. Chem.* **2007**, *72*, 6970 – 6981; c) M. Lipson, A. A. Deniz, K. S. Peters, *J. Am. Chem. Soc.* **1996**, *118*, 2992 – 2997.

[39] a) S. Shaik, D. Kumar, S. P. de Visser, *J. Am. Chem. Soc.* **2008**, *130*, 10128 – 10140; b) S. Shaik, W. Z. Lai, H. Chen, Y. Wang, *Acc. Chem. Res.* **2010**, *43*, 1154 – 1165; c) S. Shaik, P. Milko, P. Schyman, U. Dandamudi, H. Chen, *J. Chem. Theory Comput.* **2011**, *7*, 327 – 339.

[40] a) R. Latifi, M. Bagherzadeh, S. P. de Visser, *Chem. Eur. J.* **2009**, *15*, 6651 – 6662; b) S. P. de Visser, *J. Am. Chem. Soc.* **2010**, *132*, 1087 – 1097.

[41] The empirical VB (EVB) model is the basis of understanding and modeling enzymatic reactions, see, for example, a) A. Warshel, R. M. Weiss, *J. Am. Chem. Soc.* **1980**, *102*, 6218 – 6226; b) J. Aaqvist, A. Warshel, *Chem. Rev.* **1993**, *93*, 2523 – 2544.

[42] For a recent VB coupled with QM/MM see: a) A. Sharir-Ivry, H. A. Crown, W. Wu, A. Shurki, *J. Phys. Chem. A* **2008**, *112*, 2489 – 2496; b) A. Shurki, H. A. Crown, *J. Phys. Chem. B* **2005**, *109*, 23638 – 23644.

[43] For the use of MO theory to derive VB information and reactivity diagrams, see; Y. Mo, S. D. Peyerimhoff, *J. Chem. Phys.* **1998**, *109*, 1687 – 1697; Y. Mo, J. Gao, *J. Comput. Chem.* **2000**, *21*, 1458 – 1469.

[44] a) J. J. Zheng, Y. Zhao, D. G. Truhlar, *J. Phys. Chem. A* **2007**, *111*, 4632 – 4642; b) J. J. Zheng, D. G. Truhlar, *J. Chem. Theory Comput.* **2007**, *3*, 569 – 582; c) A. Dybala-Defratyka, P. Paneth, J. Z. Pu, D. G. Truhlar, *J. Phys. Chem. A* **2004**, *108*, 2475 – 2486; d) B. C. Garrett, D. G. Truhlar, *J. Chem. Phys.* **1983**, *78*, 4400 – 4413.

[45] D. G. Truhlar, J. L. Gao, C. Alhambra, M. Garcia-Viloca, J. Corchado, M. L. Sanchez, J. Villa, *Acc. Chem. Res.* **2002**, *35*, 341 – 349.

[46] W. Wu, P. Su, P. C. Hiberty, S. Shaik, *Chem. Rev.* **2011**, *111*, 7557 – 7593.

[47] B. Braida, C. Walter, B. Engels, P. C. Hiberty, *J. Am. Chem. Soc.* **2010**, *132*, 7631 – 7637.

[48] S. Shaik, P. C. Hiberty, *Comput. Mol. Sci.* **2011**, *1*, 18 – 29.

[49] a) A. P. Bento, F. M. Bickelhaupt, *J. Org. Chem.* **2008**, *73*, 7290 – 7299; b) G. T. de Jong, F. M. Bickelhaupt, *ChemPhysChem* **2007**, *8*, 1170 – 1181; c) W.-J. van Zeist, F. M. Bickelhaupt, *Org. Biomol. Chem.* **2010**, *8*, 3118 – 3127.

[50] a) D. H. Ess, K. N. Houk, *J. Am. Chem. Soc.* **2007**, *129*, 10646 – 10647; b) D. H. Ess, K. N. Houk, *J. Am. Chem. Soc.* **2008**, *130*, 10187 – 10198.

[51] a) K. Kitaura, K. Morokuma, *Int. J. Quantum Chem.* **1976**, *10*, 325 – 340; b) T. Ziegler, A. Rauk, *Inorg. Chem.* **1979**, *18*, 1558 – 1565; c) F. M. Bickelhaupt, E. J. Baerends, *Rev. Comput. Chem.* **2000**, *15*, 1 – 86; d) for a quantitative treatment of closed-shell/radical interactions, see: F. M. Bickelhaupt, A. Diefenbach, S. P. de Visser, L. J. de Koning, N. M. M. Nibbering, *J. Phys. Chem. A* **1998**, *102*, 9549 – 9553.

[52] a) As discussed in Ref. [35e], pp. 122, 155, 178, and in Ref. [34c], direct correlation of the states leads to $G = 0.75\Delta E_{ST}$, which for a C–H bond is equal to 2 *D*. A discussion is given the Supporting Information; b) See Ref. [35e] pp. 141–144 and 181–182 and in Ref. [34c,d] and also the Supporting Information.

[53] For ways to express *B*, see: a) S. S. Shaik, E. Duzy, A. Bartuv, *J. Phys. Chem.* **1990**, *94*, 6574 – 6582; b) S. Shaik, A. C. Reddy, *J. Chem. Soc. Faraday Trans.* **1994**, *90*, 1631 – 1642; c) For use of the averaged *B* expression, see Equation (3.26) in, S. Shaik, P. C. Hiberty, *Adv. Quantum Chem.* **1995**, *26*, 100 – 163.

[54] See discussions, see: G. C. Schatz, *J. Phys. Chem.* **1990**, *94*, 6157 – 6164; D. M. Neumark, *Acc. Chem. Res.* **1993**, *26*, 33 – 39.

[55] a) For the identity barrier of CH_3/CH_4 see: G. A. Creak, F. S. Dainton, K. J. Ivin, *Trans. Faraday Soc.* **1962**, *58*, 326 – 329; value of $\Delta G^{\neq}(300\ K) \approx 20\ kcal\,mol^{-1}$ can be estimated from the data in F. S. Dainton, K. J. Ivin, F. Wilkinson, *Trans. Faraday Soc.* **1959**, *55*, 929 – 936; b) T. A. Wildman, *Chem. Phys. Lett.* **1986**, *126*, 325 – 329.

[56] a) For the identity barrier of H/H_2 see: W. R. Schult, D. J. LeRoy, *J. Chem. Phys.* **1965**, *42*, 3869 – 3873; P. Siegbahn, B. Liu, *J. Chem. Phys.* **1978**, *68*, 2457 – 2465; B. Liu, *J. Chem. Phys.* **1984**, *80*, 581 – 581; D. G. Truhlar, J. C. Horowitz, *J. Chem. Phys.* **1978**, *68*, 2466 – 2476; b) For $PhCH_2/PhCH_3$ see: R. A. Jackson, D. W. O'Neal, *J. Chem. Soc. Chem. Commun.* **1969**, 1210 – 1211 ($\Delta H^{\neq} \approx 18.7$ and $\Delta G^{\neq}(298\ K) \approx 23.4\ kcal\,mol^{-1}$); c) For HO/H_2O, see: M. K. Dubey, R. Mohrschladt, N. M. Donahue, J. G. Anderson, *J. Phys. Chem. A* **1997**, *101*, 1494 – 1500.

[57] T. Uchimaru, A. K. Chandra, S. Tsuzuki, M. Sugie, A. Sekiya, *J. Comput. Chem.* **2003**, *24*, 1538 – 1542.

[58] P. W. Seakins, M. J. Pilling, *J. Phys. Chem.* **1992**, *96*, 9847 – 9855.

[59] a) A. Bassan, M. R. A. Blomberg, P. E. M. Siegbahn, L. Que, Jr., *Chem. Eur. J.* **2005**, *11*, 692 – 705; b) H. Hirao, D. Kumar, L. Que, Jr., S. Shaik, *J. Am. Chem. Soc.* **2006**, *128*, 8590 – 8606.

[60] C. B. Brewer, J. A. Peterson, *J. Biol. Chem.* **1988**, *263*, 791 – 798.

[61] a) J. Rittle, M. T. Green, *Science* **2010**, *330*, 933 – 937; b) for the experimental free energy of camphor binding in P450cam, see: S. Sligar, *Biochemistry* **1976**, *15*, 5399 – 5406; c) for experimental and theoretical values of free energy of substrate binding in P450cam, see: M. D. Paulsen, R. L. Ornstein, *Protein Eng.* **1996**, *9*, 567 – 571.

[62] D. V. Avila, C. E. Brown, K. U. Ingold, J. Luszkyk, *J. Am. Chem. Soc.* **1993**, *115*, 466 – 470.

[63] a) For a Review, see: D. V. Deubel, G. Frenking, *Acc. Chem. Res.* **2003**, *36*, 645 – 651; b) For addition of methanol to CrO_2Cl_2, see: T. Ziegler, J. Li, *Organometallics* **1995**, *14*, 214 – 223; c) For the 3+2 cycloaddition of ethylene and MnO_4^-, see K. N. Houk, T. Strassner, *J. Org. Chem.* **1999**, *64*, 800 – 802.

[64] J. P. Collman, L. M. Slaughter, T. A. Eberspacher, T. Strassner, J. I. Brauman, *Inorg. Chem.* **2001**, *40*, 6272 – 6280.

[65] J. F. Warren, T. A. Tronic, J. M. Mayer, *Chem. Rev.* **2010**, *110*, 6961 – 7001.

[66] J. H. B. Chenier, J. A. Howard, *Can. J. Chem.* **1975**, *53*, 623 – 627.

[67] T. Strassner, K. N. Houk, *J. Am. Chem. Soc.* **2000**, *122*, 7821 – 7822.

[68] J. R. Bryant, PhD Thesis (UMI number 3072066), The University of Washington, Seattle, WA, **2002**, p. 82.

[69] The $^3/_4$ factor in ΔE_{ST} is because in a perfect state correlation the spin pairing of the CrO triplet to H$^{\bullet}$ reduces the excitation by $0.25\,\Delta E_{ST}$. See, for example, S. Shaik, P. C. Hiberty, *Rev. Comput. Chem.* **2004**, *20*, 1 – 100. See especially the Eqs. (68) and (69) therein, and their explanations. Further details are in the Supporting Information.

[70] a) R. M. Miller, D. S. Tinti, D. A. Case, *Inorg. Chem.* **1989**, *28*, 2738 – 2743; b) C. L. Lasko, R. M. Miller, D. S. Tinti, *Chem. Phys. Lett.* **1986**, *130*, 359 – 364.

[71] See pp. 122–124 and pp. 145–147 in Ref. [35e].

[72] a) $EA_{PhO} = 55\ kcal\,mol^{-1}$, see: J. Lind, X. Shen, T. E. Eriksen, G. Merenyi, *J. Am. Chem. Soc.* **1990**, *112*, 479 – 482; b) $EA_{PhO} = 36\ kcal\,mol^{-1}$, see: C. R. Moylan, J. A. Dodd, C.-C. Han, J. I. Brauman, *J. Chem. Phys.* **1987**, *86*, 5350 – 5357.

[73] Using the orbitals in Scheme 3, is should be noted that the ϕ_{π}^{-} orbital in PhO···H···OPh involves an antibonding interaction with the phenyl π-orbitals (see Ref. [27]) and is hence higher in

energy than the ϕ_o^- orbital, and as such it becomes the singly occupied orbital of the PhO···H···OPh transition state.

[74] G. V. Ionova, M. E. Dyatkina, *Zh. Strukt. Khim.* **1965**, *6*, 796 – 797.

[75] For a related mechanistic "mixing" see, H. Zipse, *Acc. Chem. Res.* **1999**, *32*, 571 – 578.

[76] A recent study (M. Drees, T. Strassner, *Inorg. Chem.* **2011**, *50*, 5833 – 5840) suggests that the reaction $CrO_2Cl_2/PhCH_3$ proceeds in fact on the triplet surface. Our examination shows that the open-shell singlet transition state is the lowest species.

[77] Using the new Double Hybrid (L. Goerigk, S. Grimme, *J. Chem. Theory Comput.* **2011**, *7*, 291 – 309) with scaled correlation for different spins, we get a good barrier from the singlet state (S. Grimme, S. Shaik, D. Danovich, C. Li, unpublished results).

[78] IE of a bond depends, on the BDE as well as on the IE of the radical: $IE(H{-}Y) = BDE(H{-}Y) + IE(Y^{\bullet}) - BDE(H{-}Y^{+})$.

[79] The companion Minieview by Schwarz et al., discusses the essential need for large spin density at the abstractor site, in gas phase and surface reactions. See the Minireview in this Issue: N. Dietl, M. Schlangen, H. Schwarz, *Angew. Chem.* **2012**, *124*, 5638 – 5650; *Angew. Chem. Int. Ed.* **2012**, *51*, 5544 – 5555.

[80] For an analysis of Hammett correlations, see, R. Butler, *Chem. Br.* **1989**, *25*, 997 – 998.